UC Berkeley
UC Berkeley Electronic Theses and Dissertations

Title
Spatiotemporal receptor dynamics during early T cell signaling

Permalink
https://escholarship.org/uc/item/6pk117x3

Author
Fay, Nicole Cheung

Publication Date
2014

Peer reviewed|Thesis/dissertation

eScholarship.org Powered by the California Digital Library
University of California

Spatiotemporal receptor dynamics during early T cell signaling

By

Nicole Cheung Fay

A dissertation submitted in partial satisfaction of the
requirements for the degree of
Doctor of Philosophy
in
Molecular and Cell Biology
in the
Graduate Division
of the
University of California, Berkeley

Committee in charge:

Professor Jay Groves, Co-chair
Professor John Kuriyan, Co-chair
Professor Jeremy Thorner
Professor Ellen Robey
Professor Niren Murthy

Spring 2014

Abstract

Spatiotemporal receptor dynamics during early T cell signaling

by

Nicole Cheung Fay

Doctor of Philosophy in Molecular and Cell Biology

University of California, Berkeley

Professor Jay T. Groves, Co-chair
Professor John Kuriyan, Co-chair

A given T cell receptor (TCR) can robustly discern a pathogen-derived agonist peptide amidst a myriad of background peptides, all bound to major histocompatibility complexes (MHC). This remarkable degree of discrimination is the culmination of physical operations happening at the membrane-membrane junction between a T cell and an antigen-presenting cell. In the research described in this dissertation, I applied optical methods to hybrid interfaces between a live primary T cell and a supported lipid bilayer mimicking an antigen-presenting cell (APC) surface. In this manner, I revealed a number of novel mechanisms by which ligand-receptor dynamics dictate T cell signaling output. First, a two-parameter titration of two ligands – agonist peptide-MHC and the costimulatory surface molecule CD80/B7-1 – revealed that the density of CD80 influences the TCR activation threshold. Additionally, co-presentation led to an interdependent trafficking scheme of these surface molecules that may serve to boost the effectiveness of CD80 costimulation at low agonist peptide-MHC densities and reduce spurious activation under other conditions. Second, it was possible to resolve TCR microclusters by size using a nanoparticle array embedded in the ligand-presenting bilayer. This innovative form of size-based membrane-receptor chromatography in live cells revealed that the maximal size of the TCR microclusters was regulated by engagement with MHC molecules occupied by our model agonist peptide (moth cytochrome c). T cell antigen recognition and subsequent activation was found to be unaffected by the percolation of actively signaling TCR microclusters through this nanoparticle array. Third, myosin activity was responsible for the rapid centripetal burst of TCR microclusters in the initial 60 seconds after antigen exposure. Importantly, inhibition of myosin-induced forces abolished T cell activation, a process potentially mediated by the force-tension sensor CasL. In summary, T cell response potency results from spatiotemporal coordination of a massive interconnected signaling network undergoing continuous feedback with ligand-receptor binding events.

Acknowledgements

I firmly believe time is the most precious commodity anyone has to give and I would like to thank all the people that have given me that resource in any form. I am a better person for every moment provided to me and I hope that over my lifetime I will be able to repay that gift of kindness to other people that I meet. Here are just a handful of the people who have profoundly influenced my character and I would like to show my gratitude towards:

- My undergraduate research advisors – John Kirby and Christine Payne originally recruited me to the scientific research world and fully sold me on the rigorous and rewarding process of discovering how the natural world operates. I received the best undergraduate training possible from these two faculty while I was at Georgia Tech.
- My thesis committee – John Kuriyan provided excellent biophysical direction and showed great concern for my progress. I greatly enjoyed being a graduate student instructor in his biophysical chemistry course. Jeremy Thorner was an infinite source of wisdom regarding my thesis project and gave profound insight into my dissertation. Ellen Robey and Niren Murthy were great help regarding the fields of immunology, biophysics, and bioengineering.
- My research lab – I deeply bonded with all of the past and current Groves lab members. Niña and Boryana convinced me without doubt that the T cell team was the best path for me. Pradeep, Adam, Cheng-Han, and Wu were so incredibly kind during my rotation and were always willing to show me new techniques. My lab cohort members, Mike, Geoff, Hsiung-Lin, Lee, and Chris provided unlimited entertainment during long experiments. Training Kate was one of the best experiences in the lab and I had many great conversations with Adrienne, Laurie, Yan, Lars, and Theo. The newer lab members Monatrice, Steven, Meredith and Darren will perpetuate the wonderful camaraderie that the Groves lab has always provided.
- MY PI – Jay Groves has been a wonderful research mentor and a true leader when it comes to his research group. Jay is great at empowering lab members with enough enthusiasm to keep the lab in perpetual self-motivated motion. He has an eye for picking lab members that work seamlessly together, despite coming from very diverse, interdisciplinary, backgrounds. Though he evokes the canonical expression of “an enigma, wrapped in a riddle, surrounded by mystery,” Jay’s professional and unique demeanor cultivate an ambiance unlike any other research environment. I am honored to have received my doctoral training in the Groves lab.
- My new friends – Robyn, Iris, Hanadie, Nate, and the MCB 2008 cohort members have given me a wonderful graduate school experience. All of the MCB graduate students, staff, and faculty have been very welcoming and team-oriented. Coming to UC Berkeley for my PhD was one of the best decisions I have ever made.

- My family - Mom and Dad, you two have always shown me patience and love despite my early tendency to push boundaries. Holly, you will always be my funny, reliable, big sister and little Max, your steady logic is admirable.
- My old friends - Danielle, Maciej, and Elise, you are some of the most diverse, awe-inspiring, and scrappiest bunch of people I know.
- Christopher Wagner - I am honored to have your steadfast support. Patient, kind, a great communicator, mindful of everyone's perspectives, possessing a greater cognizance of your surroundings, and a very nerdy sense of humor are only a few of your personality traits I will enjoy in many future interactions.

Table of contents

Abstract..... 1
Acknowledgements..... i
Table of contents..... iii
List of figures..... v

Chapter 1. Introduction: Initiation and modulation of membrane-proximal T cell signaling events..... 1

1.1 Introduction..... 2
1.2 T cell signal regulation by co-receptors CD28 and CTLA-4..... 2
1.3 CD28 and CTLA-4 bind CD80 / B7-1 and CD86 / B7-2 on APCs..... 3
1.3 T cell receptor microcluster organization 4
1.4 T cell receptor transport via the molecular motor myosin..... 4
1.5 Conclusion..... 5

Chapter 2. Antigen-dependence of T cell costimulatory dynamics 6

2.1 Introduction..... 7
2.2 Materials and methods..... 9
2.2.1 Reagents..... 9
2.2.2 Preparation of T cells for imaging..... 9
2.2.3 Preparing lipid bilayer..... 9
2.2.4 Calcium flux analysis..... 9
2.2.5 Visualizing cellular receptors..... 10
2.3 Results..... 10
2.3.1 High surface density CD80 is needed to increase T cell antigen sensitivity..... 10
2.3.2 Costimulation is reduced without freely-diffusing CD80..... 12
2.3.3 CD80 transport is independent of <MCC-MHC>..... 12
2.3.4 CD80 internalization depends on <MCC-MHC> and co-receptor availability..... 17
2.4 Discussion..... 18

Chapter 3. Size-Based Chromatography of Signaling Clusters in a Living Cell Membrane..... 19

3.1 Introduction..... 20
3.2 Materials and methods..... 22
3.2.1 Fabrication of gold (Au) nanodot array..... 22
3.2.2 Preparation of T cells..... 22
3.2.3 Preparation of proteins..... 22
3.2.4 Preparation of supported lipid bilayers..... 23

3.2.5 TCR tracking experiment.... 23
3.2.6 Fixed cell experiment.... 23
3.2.7 Image analysis.... 23
3.2.8 Calcium signaling experiment.... 24

3.3 Results.... 24
3.4 Discussion.... 28

Chapter 4. Myosin IIA modulates T cell receptor transport and CasL phosphorylation during early immunological synapse formation.... 30

4.1 Introduction.... 31
4.2 Materials and methods.... 32
4.2.1 Animals.... 32
4.2.2 CD4+ cell harvest.... 32
4.2.3 DNA constructs.... 32
4.2.4 Reagents.... 32
4.2.5 Retroviral transfection.... 32
4.2.6 Bilayer assembly and cell imaging.... 33
4.2.7 Calcium imaging.... 33
4.2.8 Speckle tracking and image analysis.... 34
4.3 Results.... 34
4.3.1 Myosin IIA transiently drives translocation of TCR microclusters.... 34
4.3.2 Forces applied to TCR clusters are translated to myosin IIA.... 38
4.3.3 Myosin IIA is required for Ca^{2+} influx.... 39
4.3.4 Inhibition of myosin IIA reduces association of active ZAP-70 with TCR.... 40
4.3.5 Inhibition of myosin IIA reduces CasL phosphorylation.... 41
4.4 Discussion.... 42

Chapter 5. Closing remarks.... 44

Bibliography.... 46

List of figures

Figure 1.1. CD28, CD80, and CD86 crystal structures……..... 3

Figure 2.1. Co-presentation of peptide-MHC and CD80 on a supported lipid bilayer is ideal for observing ligand-specific costimulation……..... 8
Figure 2.2. T cells show robust calcium response to MCC-MHC in presence of CD80…….... 11
Figure 2.3. T cell costimulation is reduced by spatial confinement.....13
Figure 2.4. T cell antigen sensitivity depends on CD80 surface density and mobility…14
Figure 2.5. CD80 transport is independent of MCC-MHC……..... 15
Figure 2.6. T cell receptor microcluster initial velocity was enhanced by CD80……... 16
Figure 2.7. The nanoparticle array was characterized for interparticle spacing……. 16
Figure 2.8. CD80 internalization depends on <MCC-MHC> and co-receptor availability……... 18

Figure 3.1. Schematic of cell membrane chromatography on nanodot arrays……..…21
Figure 3.2. Signaling cluster chromatography of live T cell membranes..... 25
Figure 3.3. MHC linked via Ni-NTA lipids to the supported membrane are not preclustered . ……26
Figure 3.4. Schematic of the quantitative analysis method.....27
Figure 3.5. TCR microcluster chromatography with the titration of nanodot spacing and ag–null peptide ratios…… 28

Figure 4.1. Myosin IIA transiently drives TCR translocation and actin retrograde flow in immunological synapse formation..... 35
Figure 4.2. Inhibition of myosin only affects morphology of the early immunological synapse.....37
Figure 4.3. Physical constraints on TCR microcluster translocation impede myosin IIA movements.....38
Figure 4.4. Inhibition of myosin IIA abolishes intracellular Ca^{2+} influx..... 39
Figure 4.5. Inhibition of myosin IIA reduces phosphorylation of ZAP-70 and colocalization of pZAP-70 with TCR microclusters..... 40
Figure 4.6. Inhibition of myosin IIA reduces phosphorylation of CasL..... 41

Chapter 1

Introduction: Initiation and modulation of membrane-proximal T cell signaling events

1.1 Introduction

T cells are involved in the adaptive immune system and function by scanning antigen-presenting cells (APCs) for pathogen-derived agonist peptide bound to major histocompatibility complexes (MHCs). Aside from a length restriction (class I MHC binds peptides 8-10 residues long and class II MHC binds peptides 15-24 residues long), the peptide-binding groove in an MHC has a rather loose sequence specificity, thereby permitting presentation of a variety of peptides, including strongly activating agonist peptides, non-activating self peptides and mildly activating co-agonist peptides.[1–3] When T cells misregulate the peptide recognition event there can be a hyper-immune response, such as in autoimmune diseases, or a hypo-immune response, such as in immunodeficiency diseases (*e.g.*, AIDs). Additionally, many pathogens and even cancer cells have evolved mechanisms to evade immune recognition by the TCR.[4,5] TCR binding to agonist peptide-MHC initiates a signaling cascade that involves recruitment of two protein-tyrosine kinases, LCK and ZAP-70, to the plasma membrane in the first 30 seconds. Following the ensuing increase in downstream phospho-tyrosine signaling, there is an elevation in intracellular calcium, cytokine secretion, enhanced cell survival, and proliferation of the stimulated T cell.[6] In this manner, T cells can mount an effective immune response to an array of host threats all initiated by agonist-peptide recognition by TCR.

The spatial organization of the receptor-ligand interactions within the T cell-APC contact zone, termed the immunological synapse (IS), is recognized as a key regulator of T cell signaling.[7–11] It is known that TCR, along with many other costimulatory molecules, form microclusters that coalesce into a central region of the intercellular junction commonly referred to as the central supramolecular activation cluster (cSMAC).[12–14] A peripheral (pSMAC) and distal (dSMAC) radial region also encircle the cSMAC with receptor-ligands pairs. Key molecules in the outer concentric ringed pSMAC and dSMAC include lymphocyte function-associated antigen-1 (LFA-1) bound to intercellular adhesion molecule-1 (ICAM-1) and a transmembrane protein-phosphotyrosine phosphatase (CD45), respectively. Additionally, when high agonist peptide-MHC is encountered, T cells shed TCR-rich microvesicles, presumably as a mechanism to downregulate signaling.[15] Perturbation of the cell surface architecture in the IS alters downstream signaling pathways, such as Ca^{2+} activation and phosphorylation events.[9,11,16]

Due to the complex ensemble of other ligand-receptor interactions occurring in standard cell-based APC-T cell conjugation assays, for these studies I elected to employ instead a model system developed by my dissertation mentor, Prof. J.T. Groves. In this approach, rather than a live APC, a fluid, supported lipid bilayer (SLB) containing purified molecules of interest substitute for the surface of an APC. Another advantage of the SLB-live cell membrane system is that ligand-receptor dynamics can be directly observed with single-molecule resolution during the initial ligand-receptor event by using total internal reflectance fluorescence (TIRF) microscopy. Furthermore, SLBs are amenable for the introduction of non-invasive spatial alterations or optical enhancements. This includes chromium grids to corral protein interactions, nanoparticle arrays for receptor cluster chromatography on live cell surfaces, or nanoantennas and zero mode wave guides.[17–21]

1.2 T cell signal regulation by co-receptors CD28 and CTLA-4

This sensitive recognition process is modulated by two co-receptors also on the T cell surface: the amplificatory, costimulatory receptor CD28 and the attenuating, coinhibitory receptor CTLA-4. These antagonistic co-receptors recognize the same ligand, CD80/B7-1 and CD86/B7-2, on the antigen-presenting cell (APC) surface. Additionally, CTLA-4, CD28, and TCR activate distinct but somewhat overlapping signaling cascades including Lck activation by both and TCR and CD28, and PI3K activation by all three receptors. Due to CD80's multiple ligand-receptor interactions and intracellular crosstalk, the early coordination of these membrane-proximal signaling events remains nebulous.

CD28, a disulfide-linked homodimer, is constitutively expressed at up to 10,000 molecules/cell or ~30 molecules/μm^2 on the T cell surface.[22] The CD28 homodimer has 2 ligand binding sites but can only bind one CD80/CD86-type ligand at a time due to what would be a steric clash in the membrane-proximal domains of CD80/CD86 (Fig.1B).[23] On the intracellular side, CD28 contains multiple signaling motifs including 2 proline-rich motifs that bind Lck and Itk, and a YMNM motif that binds PI3K, Gads, and Grb2.[22,24,25] Filamin-A has also been found to co-immunoprecipitate with CD28.[26] Conversely, CTLA-4 recruits phosphatases such as SHP1, SHP2 and PP2A. CTLA-4, however, can also directly bind the TCR/CD28-associated Grb/Gads and PI3K. All of these molecules are also involved in TCR signaling, though it is unclear where and when CD28 and CTLA-4 signaling molecules converge with TCR pathways to amplify or dampen immune response output.

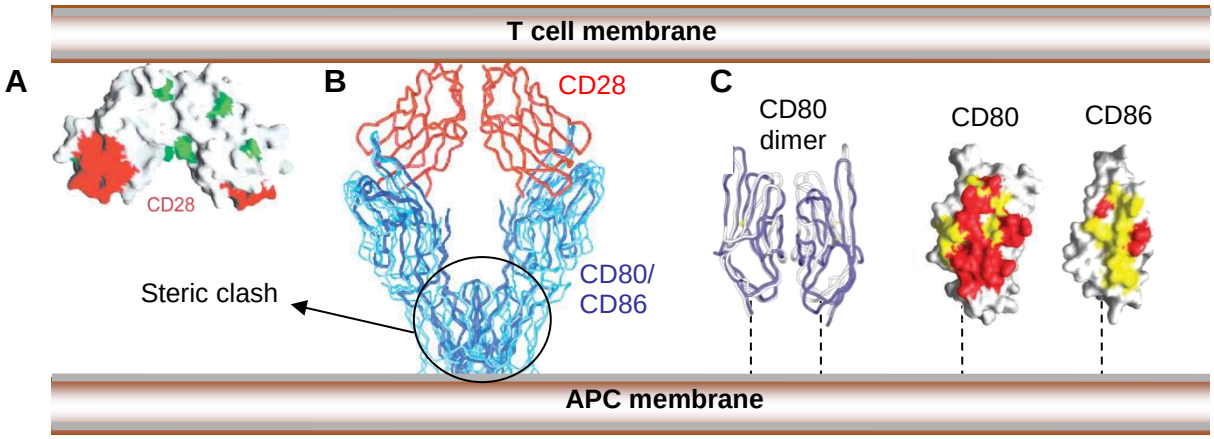


Figure 1.1. CD28, CD80, and CD86 crystal structures. CD28 forms a disulfide-linked homodimer. (A)The ligand binding site of CD28 is in red while asparagine glycosylation sites are in green. (B) CD28 has been found to be monovalent. For example, aligning a CTLA-4:CD80 and CTLA-4:CD86 based crystal structure to model CD28:CD80 binding shows that a steric clash in the CD80/CD86 ligand membrane proximal CD80 in dark blue, CD86 in pale blue). (C) CD80 and CD86 are structurally similar, in particularly the receptor-binding interface (CD80 dimer in gray, CD86 dimer in purple), however, the dimeric interface of CD80 is composed of mostly hydrophobic amino acids while the dimeric interface of CD86 is composed of hydrophilic residues (hydrophobic residues in red, hydrophilic residues in yellow). * Images adapted from Evans, E.J., et al. 2005. Nat Immunol. (A,B,D) and Zhang, X., et al. 2003. PNAS.(C).

1.3 CD28 and CTLA-4 bind CD80 / B7-1 and CD86 / B7-2 on APCs

Modulation of the initial agonist-MHC signal is dependent on CD28 and CTLA-4 binding to their cognate APC ligands, CD80/B7-1 and CD86/B7-2.[27,28] The CD80/CD86 molecules are defined as co-stimulatory because they are unable to elicit T cell activation without agonist-MHC co-presentation. However, CD80/CD86 is responsible for the majority of the T cell response to agonist-peptide.[29–31] CD80/CD86 molecules are considered a "second" signal that prevents T cell apoptosis or anergy after initial agonist peptide exposure, a fate designed to prevent unnecessary and potentially dangerous promiscuous T cell activation.[32]

The APC cell surface markers, CD80 and CD86, are structurally very similar and share 25% sequence homology with the same domain architecture.[33–35] The CD80/CD86 molecules are composed of an extracellular membrane distal variable domain as the ligand-binding site, a membrane proximal C1-set immunoglobulin super family domain, a transmembrane domain, and an intracellular cytoplasmic tail. CD80 forms a non-covalent dimer with approximately 130,000 molecules/APC while CD86 is monomeric with 60,000 molecules/APC (Fig.1C).).[22,36] Based on functional states, both CD80 and CD86 are presented at around 200 molecules/μm^2 of APC cell surface.[30] CD80 is natively a non-covalent dimer, and when presented as a covalent dimer, was determined to have a K_d of ~200 and ~12 nM for CD28 and CTLA-4, respectively.[37] Monomeric CD80 has a K_d of 4 and 0.42 μM for CD28 and CTLA-4.[38–40] CD86 was determined to have a K_d of 20 μM for CD28. Additionally, CD86 is often considered the canonical co-stimulatory molecule over CD80 due to preferential CD28 association *in vivo*, possibly because CD80 has such high affinity for the inhibitory receptor CTLA-4,.[41–43] It has also been shown that CD80 is capable of trans- and cis-binding with PD-L1 at a K_d of 1.4 μM, a potential mechanism for PD-L1's inhibition on T cell activation as PD-L1 may sequester CD80 away from CD28 binding.[44]

The newly discovered dynamics between PD-L1, CD80, and PD-1, another co-inhibitory receptor on the T cell surface that binds PD-L1, emphasize the need to resolve CD80 modes of stimulation and dynamics in a simplified system. This dissertation will investigate the mechanism of CD80 mediated costimulation during early T cell signaling using a model APC-mimetic SLB.

1.4 TCR microcluster organization

TCR dynamics on the cell surface are highly dependent on the agonist peptide density and quality.[3,7,45] The presence of agonist peptide-MHC recruits TCRs, normally randomly distributed over the T cell surface and in small intracellular pools, directly to the agonist-peptide-binding interface. At the cell-cell interface, TCRs coalesce intro microclusters that are then transported to the cSMAC. The dynamics of TCR microclusters can be resolved at the single-molecule level, however, it was previously impossible to resolve the heterogeneity of TCR microcluster sizes.

To resolve TCR microcluster formation and transport, this dissertation introduces a form of size exclusion chromatography that was imposed on the membrane of a living cell. A hexagonally ordered array of gold nanoparticles (nanodot array) was embedded

into a supported lipid bilayer displaying agonist peptide-MHC. As primary T cells interface with the proteins displayed on the bilayer, individual membrane components move freely throughout the array, while movement of larger assemblies was impeded if they exceeded the physical dimensions of the array. This technique illustrated how agonist peptide-MHC engagement dictates TCR microcluster maximal growth size.

1.4 TCR transport via the molecular motor myosin IIA

Though TCR microcluster coalescence is spontaneous upon agonist peptide-MHC ligation, the transport of the microclusters is actin-dependent.[46,47] Myosin is a well-known molecular motor known for generating the force responsible for muscle contraction. Myosin hydrolyzes ATP to drive a power stroke, enabling myosin to either walk along or pull an actin filament. Using high spatiotemporal molecular tracking studies, this dissertation characterizes non-muscle myosin IIA's role in the immunological synapse. TCR transport was driven by myosin during the first one to two minutes of a T cell interacting with the SLB. Signaling activity was also influenced by myosin activity as myosin inhibition reduces calcium influx and colocalization of active ZAP-70 (zeta-chain associated protein kinase 70) with TCR. Myosin inhibition also significantly reduced phosphorylation of the mechanosensing protein CasL (Crk-associated substrate the lymphocyte type). This implicates CasL as a potential mechanosensor in T cell signaling. Myosin's importance in T cell signaling indicates that mechanical forces also directly impact T cell response to agonist peptide-MHC.

1.5 Conclusion

There are many methods of modulating cellular response to agonist peptide-MHC. Other modes of modifying T cell antigen recognition include: crosslinking, adhesion protein interactions, other costimulatory molecules, bacterial super antigens, and viral receptor downregulation.[4,48–54] This dissertation will discuss at depth how co-receptor ligation, receptor clustering dynamics, and mechanical forces all serve to enable a robust and accurate T cell response. In this manner, the intracellular signaling network of TCR serves to fine tune and modulate T cell response during early signaling events.

Chapter 2

Antigen-dependence of T cell costimulatory dynamics

2.1 Introduction

T cells are capable of discerning extremely low numbers of agonist peptide amidst a myriad of background peptide. This highly sensitive recognition event is mediated by the T cell receptor (TCR) and triggering of an TCR can be observed on a single-molecule peptide-TCR scale.[3,55] Importantly, TCR engagement with its ligand does not represent a simple binary activation switch. T cells are capable of integrating vast amounts of information at the cell-cell interface including peptide quality, ligand-binding induced forces, and co-presentation of critical antigen-presenting cell (APC) surface markers.[1,32,56–58] This system's extreme sensitivity requires careful modulation, a feat mainly accomplished by two co-receptors also on the T cell surface: the amplificatory, costimulatory receptor CD28 and the attenuating, coinhibitory receptor CTLA-4.[28] Indeed, manipulation of these ligand-receptor interactions has shown great success in immunotherapy.[5,59] These antagonistic co-receptors recognize the same ligands, CD80/B7-1 and CD86/B7-2, on the antigen-presenting cell (APC) surface and recruit a few unique, but mostly overlapping TCR intracellular, signaling, molecules. As fitted to the name co-receptor, CD80/CD86 binding to CD28 or CTLA-4 does not begin a signaling cascade unless agonist peptide-MHC is also co-presented on the APC surface.[38]

CD28 is capable of differentially manipulating an overlapping set of TCR signaling molecules to amplify the effects of agonist peptide. CD28, when CD80/CD86 and agonist-MHC are co-presented, results in recruitment of lymphocyte-specific protein tyrosine kinase (Lck), adapter proteins Grb/Gads, phosphatidylinositol-4,5-bisphosphate 3-kinase (PI3K), and the actin-mobilization GEF protein VAV-1. CD28 costimulation affects even the earliest TCR signaling events including phosphorylation of CD3ζ, zeta-chain-associated protein kinase 70 (ZAP70), and intracellular Ca^{2+} flux. [31] CD28 is capable of recruiting filaminA, anchoring CD28 to the actin cytoskeleton network. [26] Conversely, CTLA-4 recruits phosphatases such as SHP1, SHP2 and PP2A that serve to downregulate TCR signaling. CTLA-4, however, can also directly bind the TCR/CD28-associated Grb/Gads and PI3K.

One of the main methods of regulating CD28 and CTLA-4 signaling is through varying cell protein expression and surface display. While CD28 is thought to be constitutively expressed, CTLA-4 expression is upregulated upon T cell activation, and effecter T cells keep large polarized pools of intracellular CTLA-4 that are brought to the surface upon TCR engagement with agonist peptide-MHC.[41,60]

The ligands for CD28 and CTLA-4, CD80/CD86 are presented at around 200 molecules/μm^2 of APC cell surface.[22,36] CD80/CD86 binding is characterized by low affinity and very fast association and dissociation values. CD80 is natively a non-covalent dimer, and when presented as a covalent dimer, was determined to have a K_d of ~200 and ~12 nM for CD28 and CTLA-4, respectively.[37] Monomeric CD80 has a K_d of 4 and 0.42 μM for CD28 and CTLA-4.[38–40] Additionally, CD86, though structurally similar to CD80 with the same domain architecture and 25% sequence homology, is strictly monomeric and binds with higher affinity to CD28 than CTLA-4.[33–35] It has also been shown that CD80 is capable of trans and cis binding with PD-L1 at a K_d of 1.4 μM, a potential mechanism for PD-L1's inhibition on T cell activation as PD-L1 may sequester CD80 away from CD28 binding.[44] The discovery of CD80 interactions with PD-L1 and

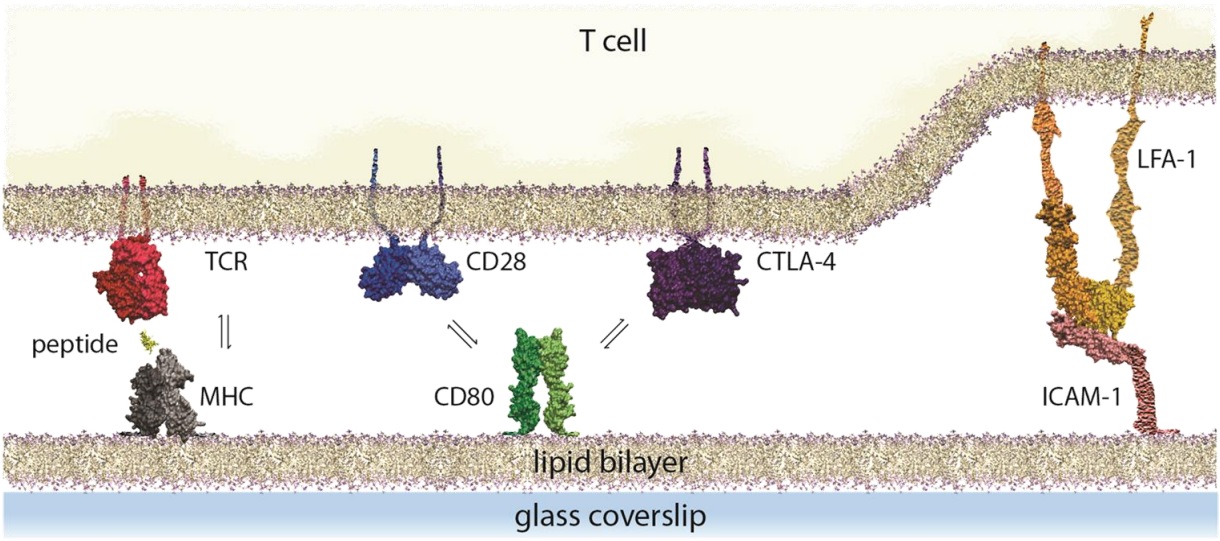


Figure 2.1. Co-presentation of peptide-MHC and CD80 on a supported lipid bilayer is ideal for observing ligand-specific costimulation. Primary AND T cells were interfaced with a supported lipid bilayer (SLB) presenting peptide-MHC, CD80 and ICAM-1. MHC was present at a constant 100 molecules/μm2 but the bound MCC agonist peptide was titrated against an inactivating null peptide (T102E). CD80 surface density was also finely tuned to enable high resolution tracking of cellular receptors, ligands, and/or calcium concentration with fluorescent indicators. To quantify molecular surface density on the bilayer, calibration curves were prepared and measured experimental intensities were compared to standard curves.

the coinhibitory T cell surface receptor, PD-1, adds another confounding variable to interpreting costimulation with standard T cell-APC conjugate assays.

Here, we have replaced the APC with a supported lipid bilayer (SLB) unambiguously displaying CD80, MHC molecules occupied by our model agonist peptide moth cytochrome c (MCC-MHC), and the adhesion protein ICAM-1, in a well defined and easy to characterize manner (Figure 1). We have quantitatively characterized the T cell dose response to varying surface densities of MCC-MHC and the costimulatory ligand CD80. CD80's costimulation enhancement was dependent on free lateral diffusion within the SLB. Using time-lapsed TIRF microscopy and a novel live-cell-membrane-cluster-size-sorting form of chromatography, we show that CD80 and TCR are not always colocalized, and in fact, the microcluster transport mechanisms work independently. Additionally, MCC-MHC binding exerts feedback in a manner that results in decreased internalization of CD80 at the cell-cell interface at low MCC-MHC. These results illustrate a novel method by which the presence of MCC-MHC induces feedback potentially to boost CD80 costimulatory effectiveness at low MCC-MHC density.

2.2 Materials and methods

2.2.1 Reagents

Recombinant proteins were expressed and purified as previously described.[9,48,61] Briefly, C-terminal decahistidine versions of ICAM-1 and CD80 were synthesized and codon optimized (Genscript) for expression in High Five (Invitrogen) insect cells via a baculovirus vector (Invitrogen). MHC Class II I-E^K with C-terminal hexahistidine tags on both α and β chains was purified from the stable insect cell S2IEK (a gift of Dr. Mark Davis, Stanford University). All proteins were purified via Ni^{2+}-NTA-agarose column (Qiagen). CD80 was labeled non-specifically with Alexa Fluor 488 or Alexa Fluor 594 (Invitrogen). H57 anti-TCR antibody fab fragments were prepared by standard protocols. All lipids were obtained from Avanti Polar Lipids. MCC peptide (88–103, ANERADLIAYKQATK) was prepared from Biosynthesis and the Dana Farber Institute.

2.2.2 Preparation of T cells for imaging

Cells were harvested and cultured as described previously.[9,62] Briefly, AND CD4+ T cells were prepared by in vitro stimulation of spleen and lymph node cells from F1 cross of ANDx B10.Br mice (Jackson Laboratory) with 1 μM MCC peptide. IL-2 was added every 48 hours along with a media change. This protocol is approved by the Animal Welfare and Research Committee under Animal Use Protocol 17702. If T cells required TCR labeling, cells were then incubated with the non-blocking antibody H57 αTCR-Fab (conjugated to Alexa Fluor 488, 594, or 647) at 4°C for 20 min.

2.2.3 Preparing lipid bilayer

Lipid bilayers on glass coverslips comprised of 98 mol% 1,2-dioleoyl-sn-glycero-3-phosphocholine (DOPC) and 2 mol% 1,2-dioleoyl-sn-glycero-3-[(N-(5-amino-1-carboxypentyl)iminodiacetic acid) succinyl] (nickel salt) (Ni^{2+}-NTA-DOGS) (Avanti Lipids) were prepared in flow chambers by standard methods.[2,9,48] MHC was loaded with agonist MCC or null (88–103, ANERADLIAYKQAEK) peptide, as indicated in the figures, 24-48 hours in advance of the experiment.[19] Bilayers were incubated with peptide-bound MHC, ICAM-1, and CD80 at room temperature for 40 minutes. Flow chambers and objectives were warmed to 37°C 10 min prior to imaging.

2.2.4 Calcium flux analysis

Intracellular calcium was observed using the ratiometric fluorescent calcium indicator fura-2-acetoxymethyl (FURA). Cells were incubated with 1 μM FURA for 15 minutes at room temperature in serum-free culture media, and then recovered for 20 minutes at 37°C in cell media with serum. For image collection, FURA was excited at 340 and 380 nm and emission collected at 510 nm via a 40xS Fluor objective on a Quantix 57 or CoolSnap K4 camera. Fields of view with or without chromium grid

patterning were monitored every 15 s for 20 min. Cell motion and fluorescence intensity were tracked and analyzed semi automatically in Imaris, Matlab, and Excel.

2.2.5 Visualizing cellular receptors

Total internal reflection fluorescence microscopy was performed on an inverted microscope (Nikon Eclipse Ti-E/B, Technical Instruments, Burlingame CA) equipped with a Nikon 100x Apo TIRF 1.49 NA objective lens, motorized Epi/TIRF illuminator, motorized Intensilight mercury lamp, Perfect Focus system, and a motorized stage (ASI MS-2000, Eugene OR). Images were recorded with an interline charged-coupled device (CCD) camera (Hamamatsu Orca-R2, Hamamatsu Japan). A 488 nm argon-ion laser (Spectra Physics 177g, Santa Clara CA), 100 mW 561 nm optically-pumped solid state laser (Coherent Sapphire, Santa Clara CA), 100 mW 640 nm diode laser (Coherent Cube, Santa Clara CA) were controlled using an acousto-optic tunable filter (AOTF) and aligned into a dual-fiber launch custom built by Solamere (Salt Lake City UT); one single-mode polarization maintaining fiber (Oz Optics, Ottowa Canada) was connected to the TIRF illuminator while the other was connected to a spinning disk confocal unit.

A spinning disk confocal head was custom fit to the microscope and camera (Yokogawa CSU-X1-M1N-E, Solamere, Salt Lake City UT). The dichroic in the spinning disk head was T405/488/568/647 multiline (Semrock, Rochester NY). Emission filters were from Chroma (Bellows Falls VT) and in a custom-mounted filter wheel (ASI FW-1000, Eugene OR): ET525/50M, ET605/52M, and ET700/75M.

Images were captured using a 1024x1 Images were acquired using Micro-Manager microscopy software. [Arthur Edelstein, Nenad Amodaj, Karl Hoover, Ron Vale, and Nico Stuurman (2010)024 pixel electron-multiplying CCD camera (Andor iXon3 888, Belfast Ireland).

2.3 Results

2.3.1 High surface density CD80 is needed to increase T cell antigen sensitivity

T cell ligand recognition was investigated in the hybrid immunological synapse system. This configuration allowed primary murine T cells to interact with a well-defined set of ligands attached to a fluid supported lipid bilayer (SLB). Non-specific presentation of stimulatory or inhibitory ligands that are normally found on antigen-presenting cells can be eliminated on SLBs, allowing for unambiguous, definitive characterization of T cell behavior. In this manner, we can investigate the specific effect of CD80-based costimulation on antigen sensitivity. SLBS were functionalized with peptide-bound MHC, CD80, and the adhesion protein ICAM-1. We could precisely control the amount of MCC-MHC and CD80 displayed on the SLB via kinetic control parameters and perform further characterization for SLB density and mobility.[61]

T cells display a robust response to increasing densities of antigen on an SLB.[2,3] Antigen recognition by TCR leads to an influx of the secondary messenger calcium. Here we have quantitatively characterized the intracellular calcium concentration, as observed via the ratiometric calcium indicator FURA-2AM, for a population of T cells as they interact with ligands on a bilayer. Reproducibility of the T cell calcium response can

be observed by comparing three replicate titrations (Figure 2.2A). Each of the MCC-MHC titrations was performed at 300 CD80 μm^{2,} and qualitatively the heat maps indicate a large population jump in the number of calcium fluxing T cells between 1 and 2 MCC-MHC/μm^2. The cellular recognition to increased antigen can be quantified by finding the average integration of every cell's intracellular calcium for a particular bilayer condition. The amount of calcium fluxed at 2 MCC-MHC/μm^2 is 1.8x the amount at 2 MCC-MHC/μm^2 (Figure 2.2B). At very high MCC-MHC, 100 molecules/μm, the active cell population shifts from 24 ± 2.1%, to 51 ±1.9%, to 86 ± 2.5% as the CD80 density is increased from 0, to 100, to 300 molecules/μm^2 (Figure 2.3A). At 1 or 2 MCC-MHC/μm^{2,} there is no significant quantified calcium flux difference between 0 and 100 CD80/μm^2 (Figure 2.3B). However, as CD80 increases to 300 molecules/μm^2, there is a 7x

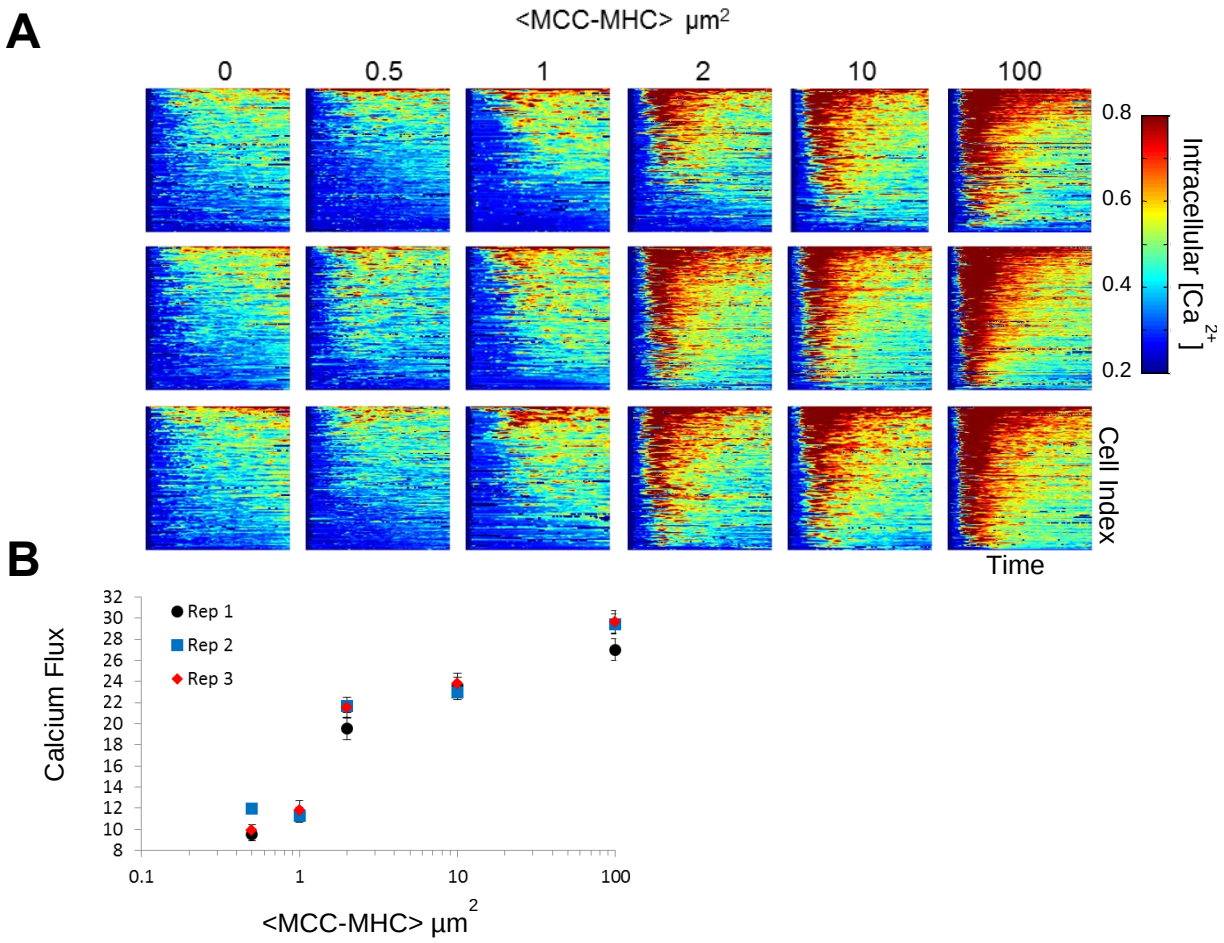


Figure 2.2. T cells show robust calcium response to MCC-MHC in presence of CD80. T cell sensitivity to MCC-MHC was observed by the intracellular [Ca2+] indicator dye FURA-2AM. Each row in a heatmap represents an individual cell's calcium response over a 20 minute period for a particular bilayer type. (**A**) Three replicates of a bilayer with 300 CD80 molecules/μm2 and varying levels of MCC-MHC were imaged. (**B**) Calcium flux is quantified by integrating the FURA-2AM 340/380 ratiometric intensity for the heatmaps shown in (**A**).

increase in the active T cell population (Figure 2.3C). The SLB represents an ideal system for investigating CD80 effects, and while the addition of a 100 CD80/μm^2 elicits minimal change in T cell calcium at low MCC-MHC, 100 CD80/μm^2 dramatically increases T cell response.

2.3.2 Costimulation is reduced without freely diffusing CD80

In order to investigate how another physical parameter, ligand lateral diffusion, might affect T cell antigen sensitivity, we patterned the SLBs with 0.5 μm chromium pitch grids. Chromium is a biologically inert metal that serves to corral SLB-bound ligands and prevent cellular transport of ligand-receptor pairs outside of the corral. Cells interacted with proteins on a SLB regardless of landing on the grid, off the grid, or on a control chromium area (Figure 2.4A). The control SLB area had chromium crosses with the same surface area as the chromium for the 0.5 μm grid, however, without the ligand confinement that a grid pattern provides (Figure 2.4B). As quantified in Figure 2.4B, T cell antigen sensitivity is reduced when cells interact with spatially confined MCC-MHC and CD80. After quantifying the calcium flux, a ~25% reduction in calcium flux is seen at 2 MCC-MHC/μm^2 + 300 CD80/μm^2 when cells are on the grid, versus the control grid. By preventing the lateral diffusion of MCC-MHC and CD80, T cells show a reduced response to MCC-MHC (Figure 2.4C). Spatial confinement decreases T cell response to higher densities of CD80 (Figure 2.3C, D).

2.3.2 CD80 transport is independent of <MCC-MHC>

The decrease in T cell response due to ligand spatial confinement leads to many questions about CD80 microcluster formation. Takashi Saito's group has done a very thorough investigation into CD28 and CTLA-4 receptor localization in the immunological synapse in this regard.[13,14] Here, I provide evidence that the microcluster transport mechanisms for MCC-MHC and CD80 occur independently, even at high MCC-MHC/μm^2. In figure 2.5A, the large central accumulation of both T cell receptor and CD80 can easily be observed at 100 MCC-MHC/μm^2. At 1 MCC-MHC/μm^2, CD80 microcluster formation and transport is also observed, despite lack of an obvious central TCR accumulation (Figure 2.5B). At 0 MCC-MHC, CD80 is still observed to undergo centripetal transport (Figure 2.5C). Thus, CD80 ligand binding and microcluster transport occurs in the absence of MCC-MHC, and does not serve to activate T cells. Additionally, further characterization of receptor inward radial velocity shows that CD80 greatly enhances the initial centripetal burst of transport by TCRs (Figure 2.6). My experiments demonstrate a stark difference in TCR and CD80 transport dependent on the MCC-MHC density.

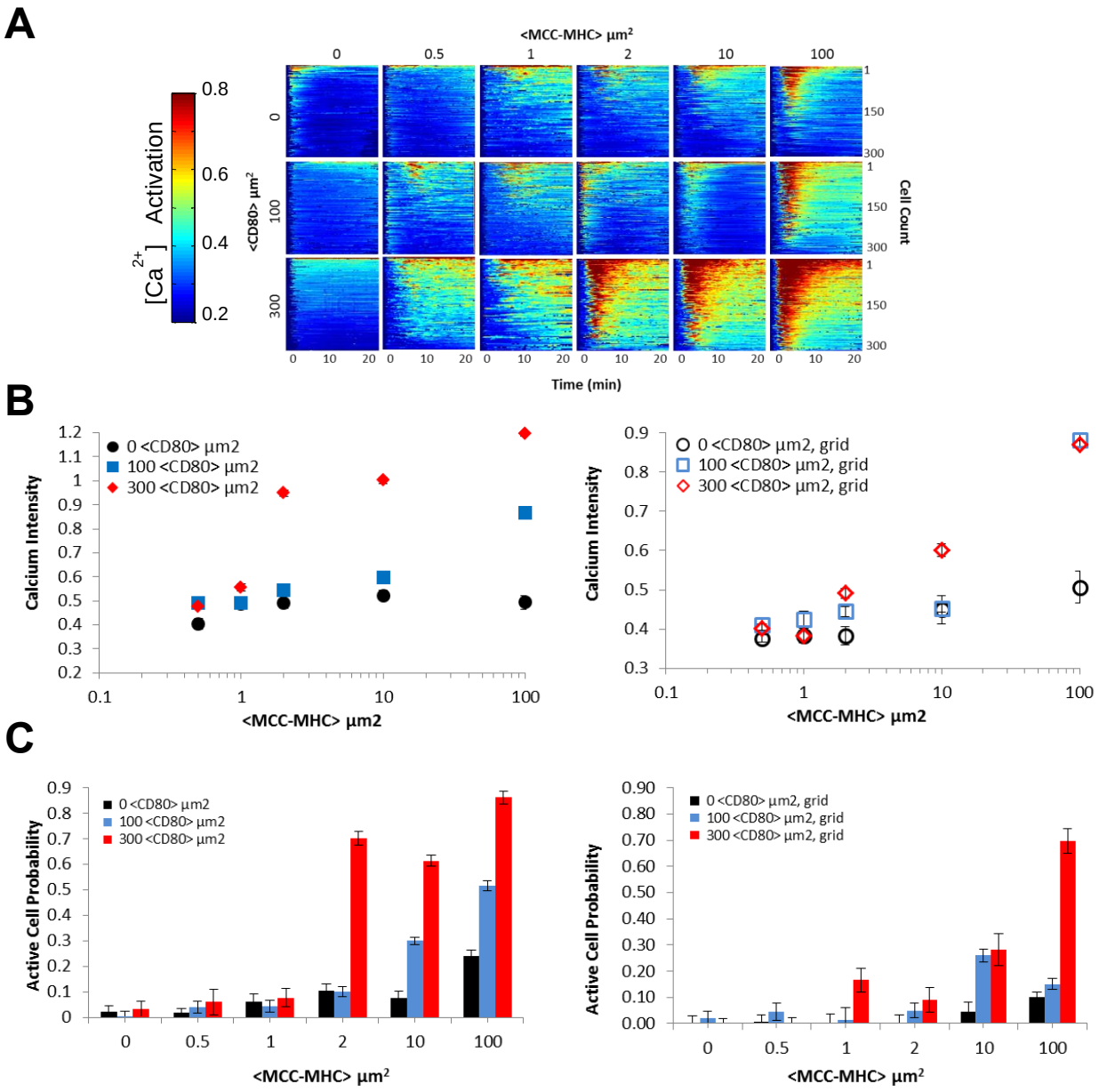


Figure 2.3. T cell antigen sensitivity depends on CD80 surface density and mobility. A two-parameter surface density titration with MCC-MHC and CD80 assayed the intracellular [Ca^{2+}] response via FURA-2. (**A**) Imaging began 15 seconds prior to the cells landing on the various bilayers and lasted for 20 min. Grid box rows (cell count) represent at least 300 cells. (**B**) The same two parameter titration was performed with additional spatial constraint of a 0.5 µm gridded SLB. Representative heat maps from the antigen sensitivity threshold are displayed. (**C**) Calcium intensity was quantified via the FURA-2AM 340/380 peak value and (**D**) the probability of T cell activation was calculated on and off grids.

Furthermore, the transport mechanism can be separated even at 100 MCC-MHC/μm^2 using a novel live-cell-membrane-cluster-size-sorting form of chromatography. This method uses gold nanoparticle arrays to parse out various sized microclusters on live cell surfaces as they are centripetally transported (Figure 2.7). Much like size exclusion chromatography, smaller clusters are able to navigate the gold nanoparticle array at a faster rate while larger microclusters stall near the periphery. Here you can see that TCR microclusters become frustrated at the cell periphery while CD80 microclusters are able to better navigate the array (Figure 2.5D). TCR and CD80 colocalization on and off the nanoparticle array further emphasizes the differential intracellular transport mechanisms (Figure 2.5D). These results indicate that despite sharing intracellular crosstalk and actin-dependence, transport of CD80 and TCR occurs independently.

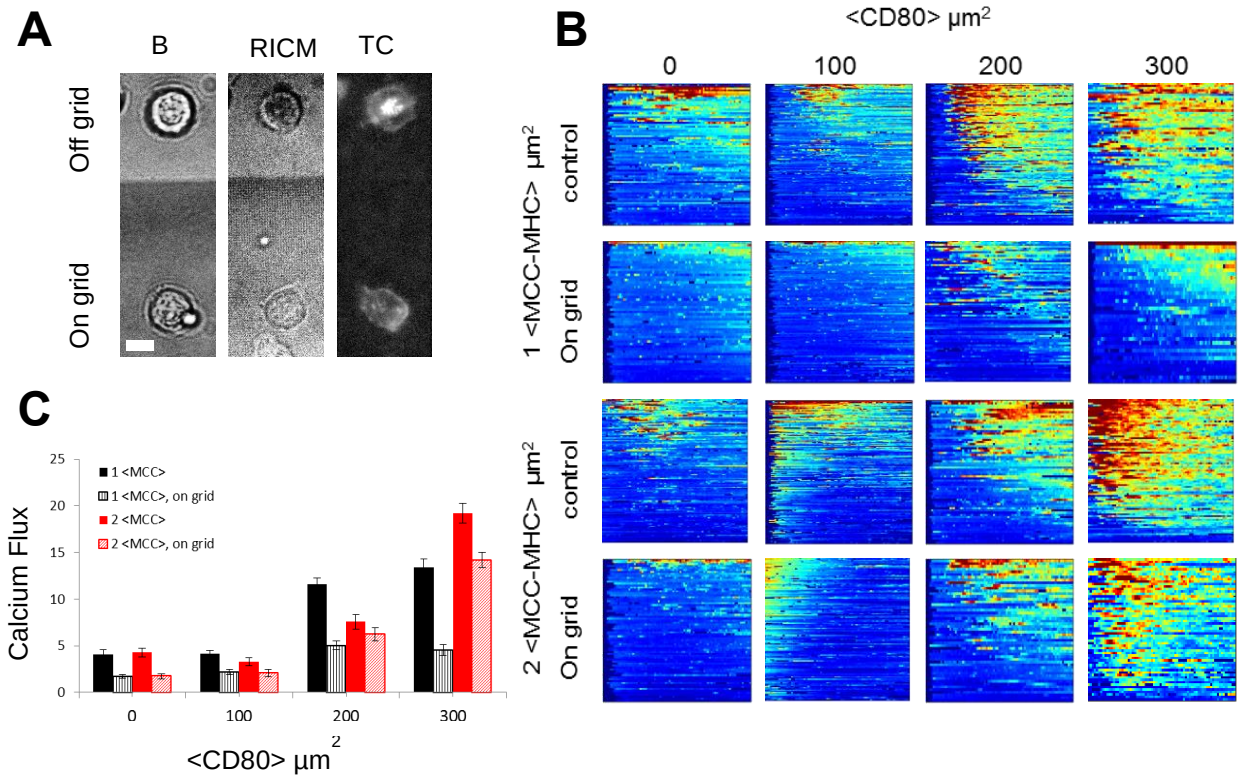


Figure 2.4. T cell costimulation is reduced by spatial confinement. T cells were deposited on chromium grids to spatially confine the presented ligands' 2d mobility. (**A**) T cells were imaged via bright-field, RICM, and fluorescent TCR while off and on the grid. Scale bar 5 μm. (**B**) CD80 surface density was titrated at the MCC-MHC threshold with cells on and off a 0.5 μm pitch gridded SLB. (**D**) Calcium flux was quantified via integrating the FURA 2AM 340/380 heatmaps shown in (**B**).

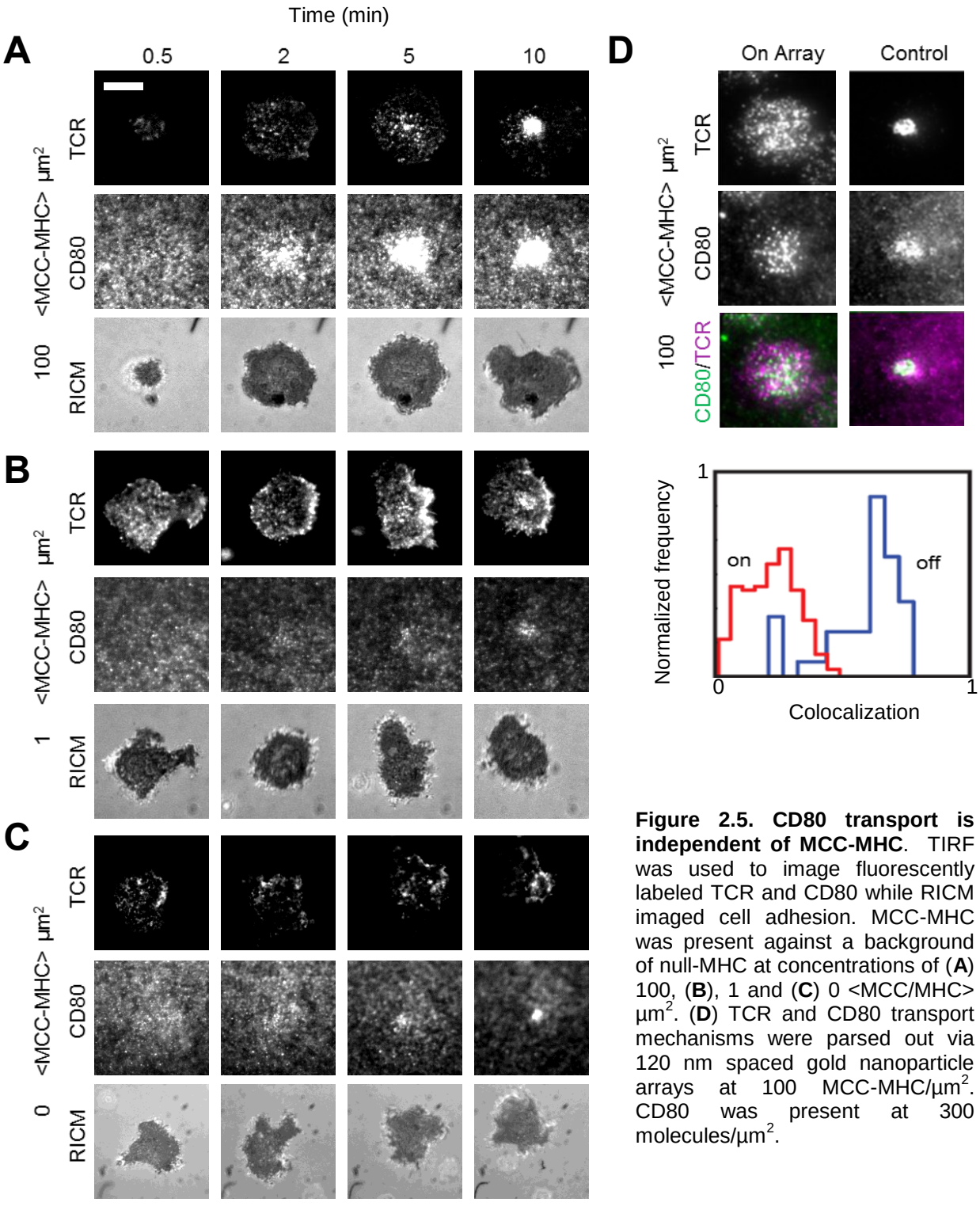


Figure 2.5. CD80 transport is independent of MCC-MHC. TIRF was used to image fluorescently labeled TCR and CD80 while RICM imaged cell adhesion. MCC-MHC was present against a background of null-MHC at concentrations of (**A**) 100, (**B**), 1 and (**C**) 0 <MCC/MHC> µm^2. (**D**) TCR and CD80 transport mechanisms were parsed out via 120 nm spaced gold nanoparticle arrays at 100 MCC-MHC/µm^2. CD80 was present at 300 molecules/µm^2.

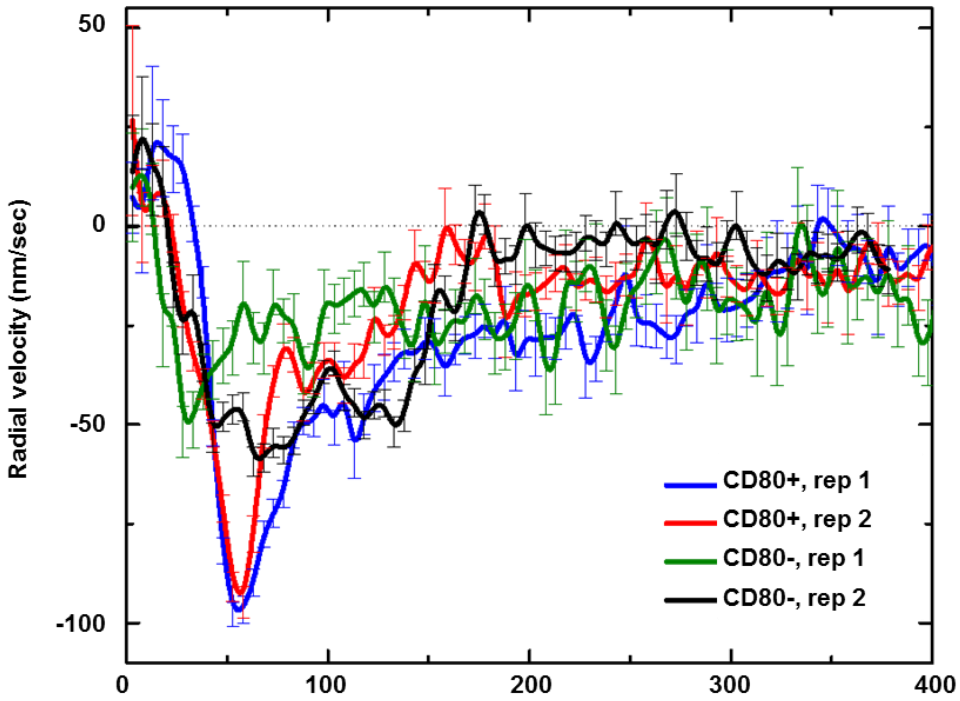


Figure 2.6. T cell receptor microcluster initial velocity was enhanced by CD80. TCR centripetal velocity was plotted for all peripheral receptor clusters on 4 cells. Blue and red indicate SLBs with CD80 while green and black were SLBs without CD80.

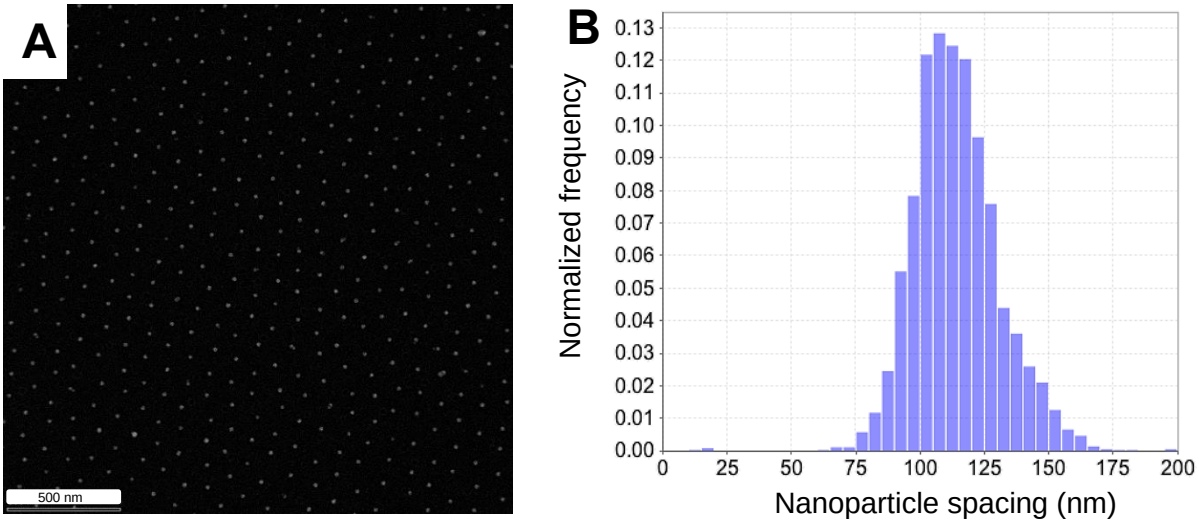


Figure 2.7. The nanoparticle array was characterized for interparticle spacing. (A) SEM images display a regular array of 5 nm gold nanoparticles. (B) The normalized frequency of the nanoparticle spacing was calculated for an array.

2.3.4 CD80 internalization depends on <MCC-MHC> and co-receptor availability

CD80 is known to be internalized by T cells when presented on APCs, however, uptake in a minimalist ligand environment has not been performed. Approximately 3.2x more CD80 particles, and with greater volume, were internalized at 0 MCC-MHC versus 100 MCC-MHC after a 20 minute period (Figure 2.8A). The presence of even 1 MCC-MHC almost entirely halted cellular uptake of CD80. A 31x fold reduction in CD80 internalization was observed at 1 MCC-MHC/μm^2 versus 0 MCC-MHC/μm^2 (Figure 2.8B). Mild CD80 internalization was observed at high MCC-MHC densities, albeit in a very heterogeneous manner. This indicates that CD80 internalization is dependent on MCC-MHC density, despite independent transport and scaffolding mechanisms.

Further investigation into the co-receptors responsible for CD80 internalization showed that blocking both CD28 and CTLA-4 abolished any uptake at 0 MCC-MHC/μm^2 (Figure 2.8C). Both CTLA-4 and CD28 were important for contributing to CD80 particle uptake by the 20 minute time point. These results indicate that CD28 may also be involved in CD80 regulation at the cell-cell interface.

2.4 Discussion

In conclusion, these experiments elucidate a unique spatiotemporal mechanism that may enable maximal CD80 costimulation at physiologically low antigen conditions. CD80 at high surface densities (300 CD80/μm^2) was required to increase T cell antigen sensitivity, a density in the upper bounds of the 200 CD80/μm^2 estimate. [22,36] This may potentially be due to CD80's higher affinity for the inhibitory receptor CTLA-4, and binding of those receptors preferentially as intracellular CTLA-4 rapidly displays on the surface in response to agonist peptide-MHC.[63] A higher number of CD80 would be required for the costimulatory CD28 to gain binding favor as CTLA-4 receptors became saturated. In this manner, retention of CD80 at the cell-cell interface is critical for enhanced T cell antigen sensitivity.

Investigation into CD80 transport mechanism reveals that the CD80 ligand does not need to be in close proximity to TCR to have a positive, costimulatory, effect. This has been observed before with the use of micropatterned antibodies.[64] Indeed, CD80 binding and transport was observed in the absence of agonist peptide. The dynamic centripetal transport of CD80 is likely necessary for the massive internalization observed when no agonist peptide is present. Internalization may serve as a "damping by depletion" method of regulating T cell activation.[65,66] Conversely, inhibition of internalization, such as observed at low agonist peptide densities, might serve to boost CD80's costimulatory effects. At high agonist peptide conditions, CD80 uptake was minimal. Instead, the massive central accumulation of CD80 and TCR at the cell-cell interface may also represent a form of down-regulation of T cell receptor-ligand pairs via microvesicle depositing.[15]

In summary, the higher CD80 surface densities necessary for enhanced antigen recognition, the mobilization of CD80 in the absence of antigen, and the agonist-induced blockade of CD80 at low antigen conditions may all serve to boost the CD80 effect overwhelmingly in favor of the positive, costimulatory receptor CD28.

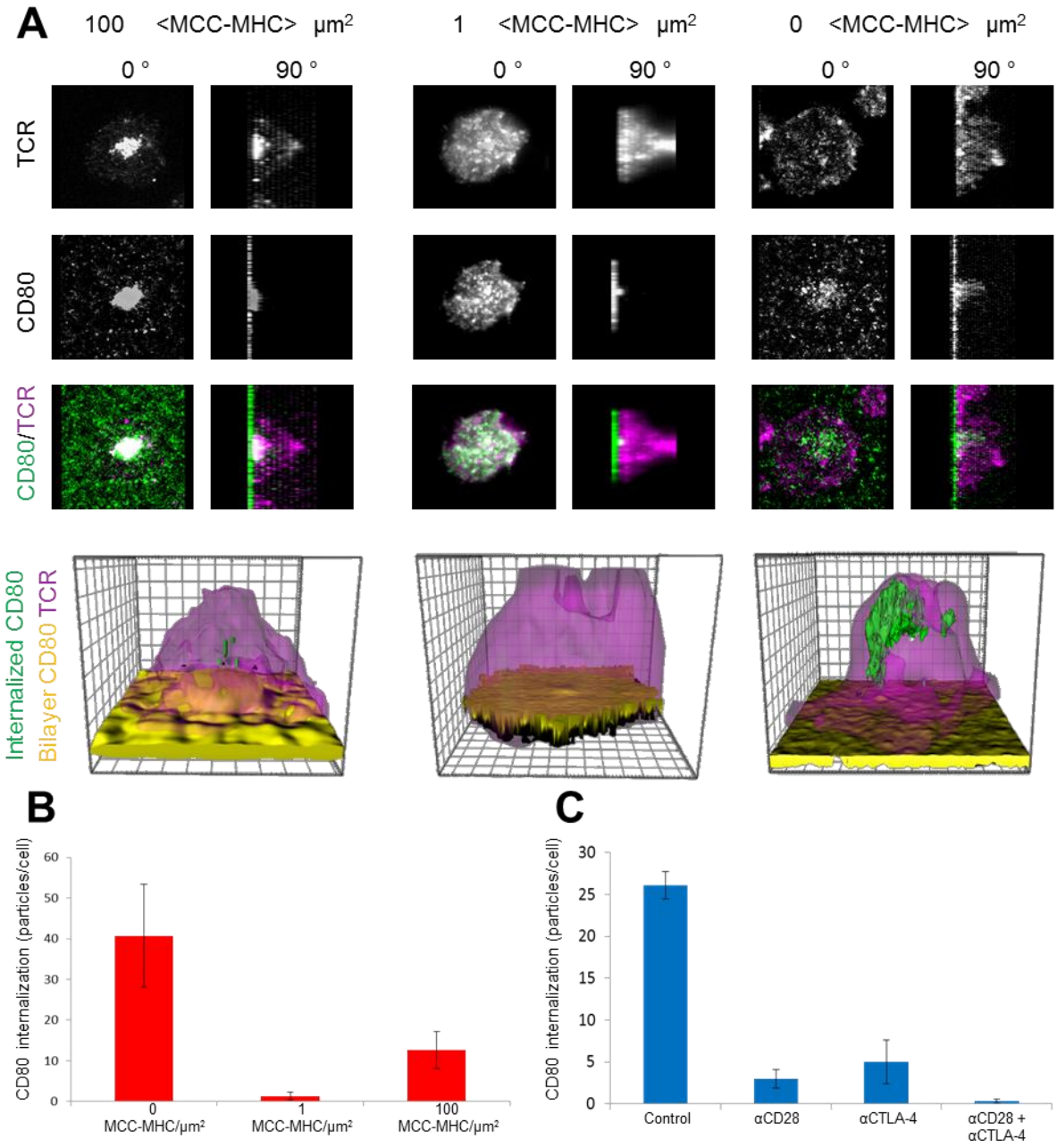


Figure 2.8. CD80 internalization depends on <MCC-MHC> and co-receptor availability. Confocal microscopy imaged TCR (magenta) and CD80 (green) after T cells were exposed to (**A**) 0, 1, or 100 MCC-MHC/µm^2 for 20min. Scale bar 5 µm. Grid frame 1 µm. (**B**) CD80 internalization was characterized for number of particles per cell. Internalization analysis was performed by removing Z-slices within 1 µm of the CD80 bilayer counting the remaining particles. (**C)** T cells were then incubated with monoclonal blocking antibodies to CD28, CTLA-4, or both at the indicated <MCC-MHC>.

Chapter 3

Size-Based Chromatography of Signaling Clusters in a Living Cell Membrane

* The work presented in this chapter has been previously published as part of the following paper: Niña G. Caculitan; Hiroyuki Kai; Eulanca Y. Liu; Nicole Fay; Yan Yu; Theobald Lohmüller; Geoff P. O'Donoghue; Jay T. Groves; *Nano Letters* (2014).

* Niña G. Caculitan, Hiroyuki Kai, and Eulanca Y. Liu equally conceived and performed the experiments, analyzed and interpreted the data, and wrote the manuscript. Nicole Fay performed the calcium-related experiments, characterization of molecular surface densities, and all of the associated analyses. Yan Yu performed the TCR tracking experiments. Theobald Lohmüller helped fabricate the gold nanoparticle arrays. Geoff P. O'Donoghue performed the single molecule photobleaching experiment.

3.1 Introduction

Cell membranes exist in a highly organized liquid state. The dynamic assembly of proteins and lipids into functional supramolecular structures within the membrane plays a foundational role in many signaling systems.[67] Although these facts are well-accepted at a general level, the physical properties of membrane substructures along with the details of how spatial organization is tied to function remain enigmatic. This is largely the result of substantial limitations to the application of optical microscopy at length scales below the 250 nm diffraction limit. Fluorescence-based super-resolution,[68–70] tracking,[71] and time correlation techniques[72,73] are beginning to probe smaller length scales. Even so, imaging alone may never be sufficient to fully reveal the dynamic physical nature of cell membranes. Supported membranes embedded with nanodot arrays,[18] which we apply here to probe T cell receptor (TCR) microclusters[74–77] in T cell membranes, represent a tactile approach to probing membrane structures in living cells. They reveal information that is distinct from optical methods and can expose physical aspects of the membrane environment unobservable by other techniques.

Cellular signal transduction often involves assembly of molecules into organized structures on the cell membrane.[67,78,79] The TCR microcluster, which is the functional module for antigen recognition by T cells, is a prototypical example. Similar assemblies are emerging in other juxtacrine signaling systems, such as the Eph receptor tyrosine kinases.[80–82] These signaling clusters occupy a size regime of tens to a few hundred nanometers and thus typically lurk below the diffraction limit of conventional optical microscopy. As such, direct information about their physical characteristics is limited.

Supported membranes functionalized with intercellular adhesion molecule-1 (ICAM-1) and peptide-loaded major histocompatibility complex (pMHC) proteins can effectively replace the antigen-presenting cell (APC) to form a hybrid immunological synapse with a living T cell.[83] As TCR on the T cell engage their antigen pMHC ligands on the supported membrane, they assemble into signaling microclusters, [74–77] which indirect estimates suggest range in size from 70 to 500 nm[74,84] (Supplementary Table S1 in the associated manuscript[19]). Within a matter of seconds after formation, the TCR microclusters become coupled to actin retrograde flow and are centripetally transported to the center of the junction to form the classical immunological synapse.[76,85,86] Physical structures, such as patterns of metal lines or arrays of gold nanodots (described here), can be fabricated onto the underlying substrate to define geometric restrictions on molecular transport in the supported membrane.[17,18] These substrate-imposed constraints are selectively transmitted to the living cell through receptor–ligand interactions to induce what we refer to as a spatial mutation.[2,9,82] In the case of the nanodot array, TCR cluster transport is impeded if the clusters are too large to percolate between individual nanoparticles in the array (Figure 3.1).

Most applications of the supported membrane spatial mutation to date have relied on electron-beam lithography to pattern the substrate.[2,9,62,82,85] While this fabrication method can achieve the necessary spatial resolution (tens of nanometers) for cellular experiments, it is prohibitively slow and expensive for many applications. Here we employ a relatively straightforward method of block copolymer nanolithography to produce ordered arrays of gold nanoparticles (5–10 nm diameter) with highly controlled (relative standard deviation <20%) interparticle spacings ranging from 40 to

180 nm (Supplementary Figures S1 and S2 in the associated manuscript[19]).[18,20,87–89] Interparticle spacings are controlled by the deposition and the specific polymers used in the gold micelle solution (Supplementary Table S2 in the associated manuscript[19]). Nanodot arrays can be readily fabricated over cm2 areas, and supported membranes subsequently assembled on the substrate exhibit free mobility (D 1 μm2/s)[18,90] throughout the array (Supplementary Figure S3 in the associated manuscript[19]).

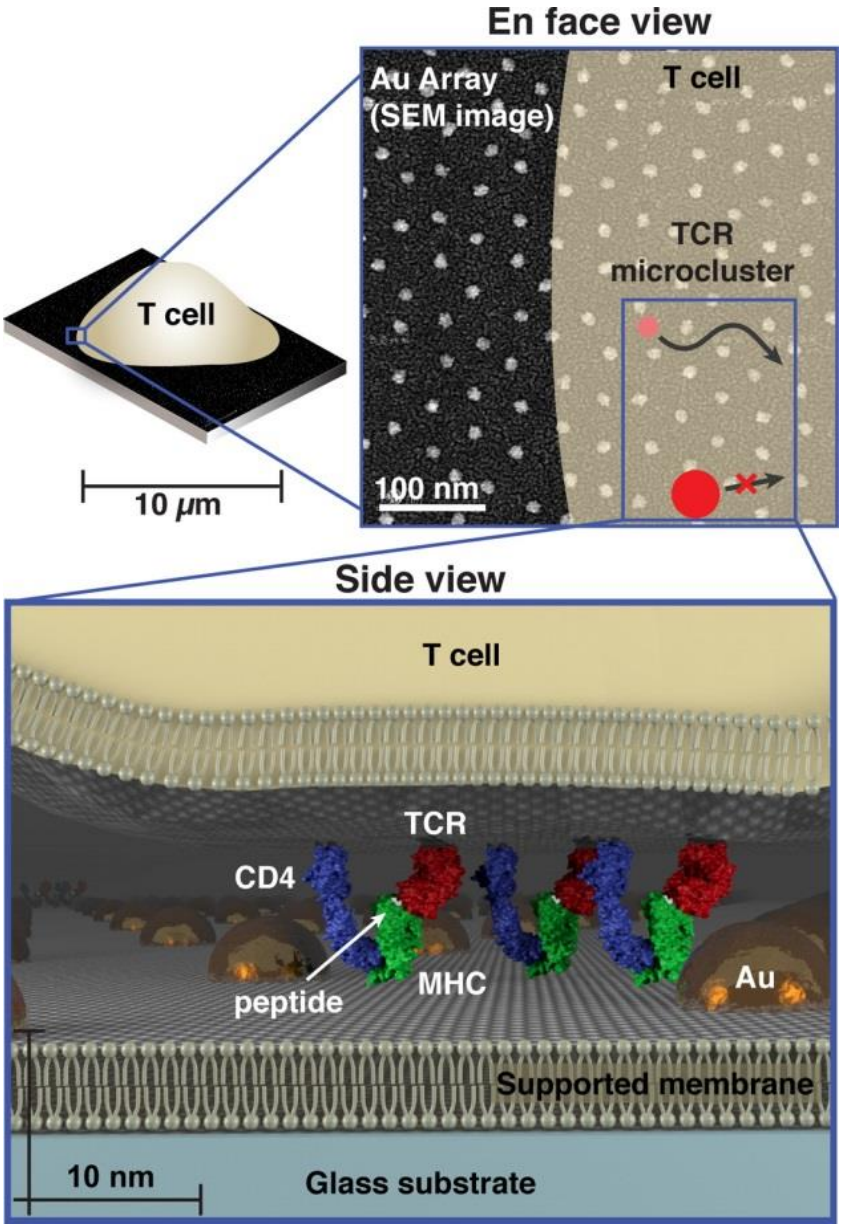


Figure 3.1. Schematic of cell membrane chromatography on nanodot arrays. (Top) Scanning electron micrograph of an array with 40 nm spacing superimposed with a schematic of a T cell outline and TCR signaling microclusters. TCR microclusters smaller than the spacing exhibit no restriction in centripetal transport, while the transport of larger microclusters is impeded. (Bottom) 3D scale schematic of a T cell interaction with a functionalized supported membrane containing an embedded nanodot array. TCR (red) on the live cell interacting with pMHC (green) molecules is illustrated. Intermembrane spacing between the T cell and supported membrane within TCR microclusters is much closer than elsewhere in the cell. Other TCR microcluster proteins, such as CD4 (blue), may also interact with the nanodot array. These specific interactions allow the array to probe physical properties within the living T cell membrane.

3.2 Materials and methods

3.2.1 Fabrication of gold (Au) nanodot array

Au nanodot arrays were deposited on glass substrates according to the method previously reported[18]. In addition, the array with 40 nm spacing was fabricated as follows. Toluene (60.5 mL, Sigma-Aldrich) was added to PS-b-P2VP (Mn(PS) = 7.9 × 104, Mn(PVP) = 3.65 × 104; 302 mg, 2.6 μmol, Polymer Source) in a capped glass vial and the mixture was stirred overnight at room temperature for complete dissolution. Chloroauric acid hydrate (HAuCl4) (Sigma-Aldrich, 154.2 mg, 0.45 mmol; [HAuCl4]/[VP]PVP = 0.50) was added to the polymer solution and stirred overnight at 40°C. Glass coverslips (diameter = 40 mm, Bioptechs) were sonicated in IPA/water for 30 min, rinsed with water, and immersed in piranha solution (H2O2:H2SO4 = 1:3) for 15 min. Coverslips were then rinsed copiously with water and dried with a stream of nitrogen gas. Within 45 min, one-half of the substrate was dip-coated in the Au micelle solution. The substrate was then plasma irradiated using a plasma cleaner (PDC-32G, Harrick Plasma) operated at 18 W for 90 min to remove the polymer and reduce the Au salt to form the nanodot array. Sample substrates from each batch were imaged by scanning electron microscopy (SEM) on a Hitachi S-5000 operated at 10 kV acceleration voltage. Interparticle spacing was calculated using particle detection by threshold on ImageJ followed by nearest neighbor detection by Delaunay triangulation algorithm[91] (Fig. S1 in the associated manuscript[19]; Source code is available at https://github.com/hirokai/Delaunay). Polymers and dip-coating speeds were varied accordingly for different spacings (Table S2).

3.2.2 Preparation of T cells

AND CD4+ T cells were harvested from lymphocytes and splenocytes of F1 generation AND × B10.Br mice (Jackson Laboratory) 6-13 weeks of age and expanded to T cell blasts as previously described.[9] This protocol is approved by the Animal Welfare and Research Committee (AWRC) under Animal Use Protocol #177002.

3.2.3 Preparation of proteins

Histidine-tagged intercellular adhesion molecule-1 (ICAM-1) and major histocompatibility complex (MHC) Class II I-Ek proteins were expressed and purified as before.[92] Fab fragments derived from H57 anti-T cell receptor (TCR) antibodies were prepared by standard protocols. Moth cytochrome c (MCC) agonist peptide (ANERADLIAYLKQATK) and/or T102E (ANERADLIAYLKQAEK) null peptide were loaded onto MHC at 100 μM in pH 4.5 citrate buffer and incubated at 37°C 48 hours prior to pMHC incubation with the supported lipid bilayer (supported membrane). For pMHC imaging experiments, MCC-C (ANERADLIAYLKQATKGGSC) was used instead of MCC. Conjugation of ICAM-1 with Alexa Fluor 488 (AF488), anti-TCR Fab with Alexa Fluor 594 (AF594), and MCC-C with Alexa Fluor 488 maleimide was performed according to Molecular Probes instructions.

3.2.4 Preparation of supported lipid bilayers

Substrates with the Au nanodot array prepared above were irradiated with air plasma for 5 min to activate the surface and were used as the bottom face of an enclosed, temperature-controlled flow cell system (FCS2, Bioptechs). The entire surface was covered with a supported membrane spontaneously formed with the addition of small unilamellar vesicles of 1,2-dioleoylphosphotidylcholine (DOPC) containing 2 mol% 1,2-dioleoyl-sn-glycero-3-[(N-(5-amino-1-carboxypentyl) iminodiacetic acid) succinyl] (nickel salt) (Ni-DOGS) (Avanti Polar Lipids) prepared by standard methods.[90] ICAM-1 and pMHC were loaded on the supported membrane with a 40 min incubation at room temperature followed by a 1x tris buffered saline solution rinse to wash away unbound proteins. For ag:null titration experiments, ag pMHC and null pMHC solutions were added according to the ratios indicated.

3.2.5 TCR tracking experiment

Primary murine T cells were incubated with AF594 anti-TCR Fab fragments for 20 min on ice, then injected into the flow cell at 37°C containing the supported membrane prepared above. Total internal reflection fluorescence (TIRF) microscopy images were taken using Orca-R2 CCD camera (C10600-10B, Hamamatsu Photonics K.K.) with a 561 nm laser source (GCL-100-561, CrystaLaser) at a rate of 1 s-1 with 500 ms exposure time. Particle tracking of the images was performed using a MATLAB script[86] and u-track software.[93]

3.2.6 Fixed cell experiment

T cells were stained and incubated with the supported membrane as above at 37 °C for 20 min, then fixed with 2% paraformaldehyde for 10 min. Cells were then imaged using a 100x oil immersion objective and corresponding filter cubes. Epifluorescence images were captured using CoolSNAP HQ CCD camera (Photometrics) using MetaMorph software package (Molecular Devices). TIRF images were captured using Orca-R2 CCD camera with 488 nm argon-ion laser (177g, Spectra Physics) and 561 nm optically-pumped solid state laser (Coherent Sapphire) as the laser sources.

3.2.7 Image analysis

The radial profile of the TCR image of every cell was calculated by a program that was developed on the ImageJ platform. (http://github.com/hirokai/TCRAnalysis). Variance of the radial profile of every cell, σ2, is defined for the symmetrized radial profile, P(r), by the equation,

$$\sigma^2 \equiv \int_{-1}^{1} r^2 P(r)dr, \text{where } P(r) \equiv \frac{p(|r|)}{2} . \left(\int_{-1}^{1} P(r)dr = 1 , \int_{-1}^{1} rP(r)dr = 0 \right)$$

Radial profiles were averaged over all the cells (n ≥ 39, typically n > 100) on and off the nanodot array respectively. Variance of the radial profile was collected to plot a histogram, and analyzed by R software for statistical significance.

3.2.8 Calcium signaling experiment

Non-fluorescent ICAM-1 was loaded onto the supported membrane along with pMHC as described above. Cells were first incubated with 1 μM fura-2-acetoxymethyl ester (Fura-2 AM, Molecular Probes) in FBS-free media for 15 min at room temperature and incubated with serum rich media at 37°C for 20 min. Cells were then labeled with AF594 anti-TCR antibody as above. Intracellular calcium flux was monitored with excitation wavelengths of 340 and 380 nm and emission of 510 nm using a 40x objective with CoolSnap K4 camera as before.[61] Time course of Fura-2 340/380 fluorescence intensity ratio of every cell was analyzed by Imaris software and the intensity profiles were plotted as heat maps by a MATLAB script.

3.3 Results

Nanodot arrays differentially restrict long-range transport of TCR microclusters as a function of the interparticle spacing within the array. TCR on primary AND T cells were labeled with a fluorescent anti-TCR H57 fab fragment, which does not interfere with pMHC-TCR binding.[74] As TCR engage pMHC loaded with activating agonist peptide moth cytochrome C (MCC; ANERADLIAYLKQATK) in the supported membrane, signaling clusters form, and their movement was tracked on live cells by total internal reflection fluorescence (TIRF) microscopy (Figure 2a and b). On a 171 nm spaced array with an average agonist pMHC density of 80 molecules/μm2 (Supplementary Figure 4 in the associated manuscript[19]), most TCR clusters successfully percolate through the array. The final positions of continuously tracked clusters are circled on both the track plot (top) and final frame (bottom) in Figure 3.2a. On a 40 nm array with the same agonist pMHC density, clusters exhibit some centripetal transport but most become trapped while still in peripheral positions (Figure 3.2b). In general, agonist pMHC is observed to colocalize with TCR, irrespective of whether they are freely moving or trapped (Figure 3.2c, d and Supplementary Figure S5 in the associated manuscript[19]). Leukocyte function associated antigen-1 (LFA-1) bound to ICAM-1 can still form a ring pattern, as is characteristic in a mature immunological synapse (Supplementary Figure S6 in the associated manuscript[19]). This suggests that LFA-1:ICAM-1 complexes are less affected by the physical constraints imposed by the nanodot arrays. In addition to the larger lateral size of TCR microclusters, as compared with LFA-1:ICAM-1 clusters,[48] the closer apposition of the two cell membranes dictated by the short length of the pMHC:TCR complex[56,94,95] is likely to also contribute (see, for example, Figure 1).

Although the 40 nm spaced nanodot array impedes long-range transport of TCR clusters, no significant interference with signaling function was observed (Supplementary Discussion 1 in the associated manuscript[19]). To quantitatively characterize the antigen specific triggering of T cells, we monitor intracellular Ca2+ flux using a Fura-2 dye reporter[2] while titrating the ratio of agonist peptide to a null peptide (T102E) at constant total pMHC density (80 molecules/μm2). Null peptide-pMHC alone does not induce TCR triggering. The Ca2+ concentration (colorimetric scale) is plotted for each cell (y-axis) as a function of time (x-axis) (Supplementary Figure S7 in the associated manuscript[19]) for at least 350 cells per condition in Figure 3.2e. Agonist–null

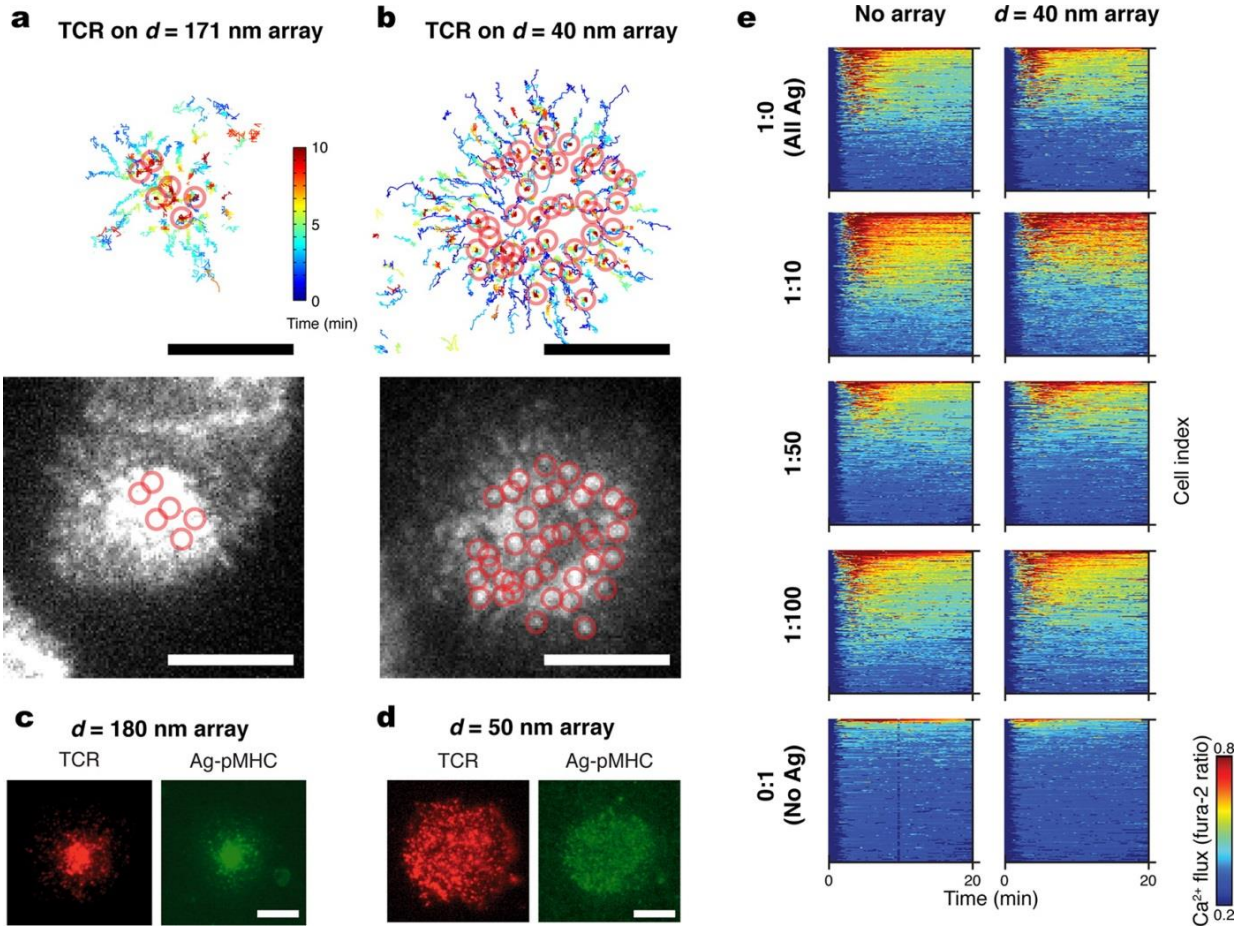


Figure 3.2. Signaling cluster chromatography of live T cell membranes. (Top **A,B**) Individual trajectories of TCR microclusters in cells interacting with supported membranes containing nanodot arrays of (**A**) 171 nm or (**B**) 40 nm spacing. Color bar represents elapsed time (0–10 min). Open circles indicate final positions. (Bottom a,b) TIRF images of the cells after 10 min. (**C, D**) Epifluorescence images of TCR (red) on cells interacting with pMHC (green) presented on a SLB studded with 180 nm spacing (**C**) or 50 nm spaced (**D**) arrays. (**E**) Intracellular Ca2+ flux for cells presented with varying ratios of agonist (ag) to null peptide presented by pMHC on SLBs with or without the nanodot array; nanodot arrays do not interfere with T cell triggering. Scale bars: 5 μm.

ratios from 1:0 to 1:100 all lead to comparable Ca2+ response in T cells on or off the arrays. When no agonist peptide is present, essentially no Ca2+ response is observed in either case.

T cells can respond to fewer than 10 individual agonist peptides.[2,3,55] However, morphological characterization of the immunological synapse and TCR signaling cluster phenomena is often performed at agonist pMHC densities in the range of 2000–15000 per cell.[75,83] Little is known about how the physical properties of TCR signaling clusters scale with antigen density or even if stable TCR clusters exist at the lowest level of antigens that can lead to T cell triggering.[2,76] This is especially important given that, under most physiological conditions, antigen is present on cell surfaces at extremely low levels. Here we apply the nanodot array chromatographic strategy to probe the physical properties of TCR signaling clusters as a function of antigen density.

To ensure homogeneous distribution of monomeric pMHC on the supported membrane, proteins are tethered via polyhistidine linkage to nickel-chelating lipids within a background of 1,2-dioleoylphosphotidylcholine (DOPC) lipids.[61] This strategy does not lead to preclustering, as is clearly indicated by direct single molecule imaging of peptide-labeled pMHC complexes in supported membranes (Figure 3.3 and Supplementary Figure S8 in the associated manuscript[19]). We note that GPI-linked pMHC, which was used in a number of earlier studies,[9,62,96] has been shown to exhibit self-clustering tendencies in supported membranes[2,76] (Supplementary Discussion 2 in the associated manuscript[19]).

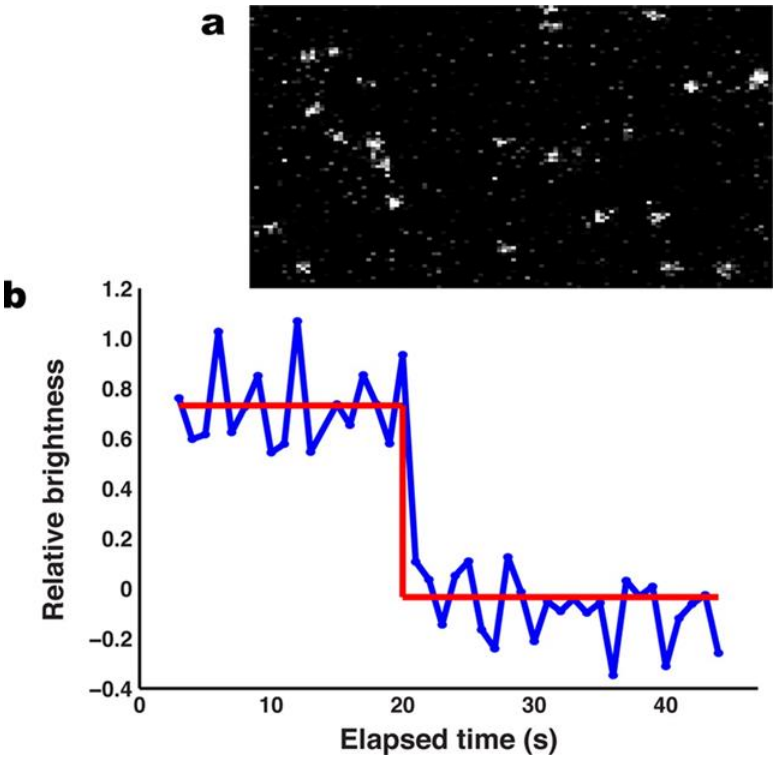


Figure 3.3 MHC linked via Ni-NTA lipids to the supported membrane are not preclustered. (**A**) TIRF image of a bilayer presenting MHC loaded with Atto647N-labeled MCC(C). (**B**) Collection of single molecule traces for individual pMHC molecules. The red line denotes intensity levels detected using a Bayesian change point technique(7) and a Bayes Factor of 25. Data were collected at 17.5 ms intervals. Discrete single-step photobleaching observed for all molecules indicates that the pMHC exists ~100% as a monomer.

The relative frustration of TCR cluster transport induced by the nanodot array can be quantified using a radial profile analysis as depicted in Figure 3.4. The measured TCR density is converted into a normalized radial probability distribution. We compute the variance, σ2, of the symmetrized probability distribution to provide a scalar measure of the degree of frustration (Methods in the Supporting Information in the associated manuscript[19]). In an uninhibited immunological synapse, the radial transport of TCR toward the geometric center of the junction leads to low variance while a completely frustrated system exhibits high variance. This analysis allows comparison of cells as well as analysis of cell–cell variation within an ensemble unbiased by labeling efficiency or cell size.

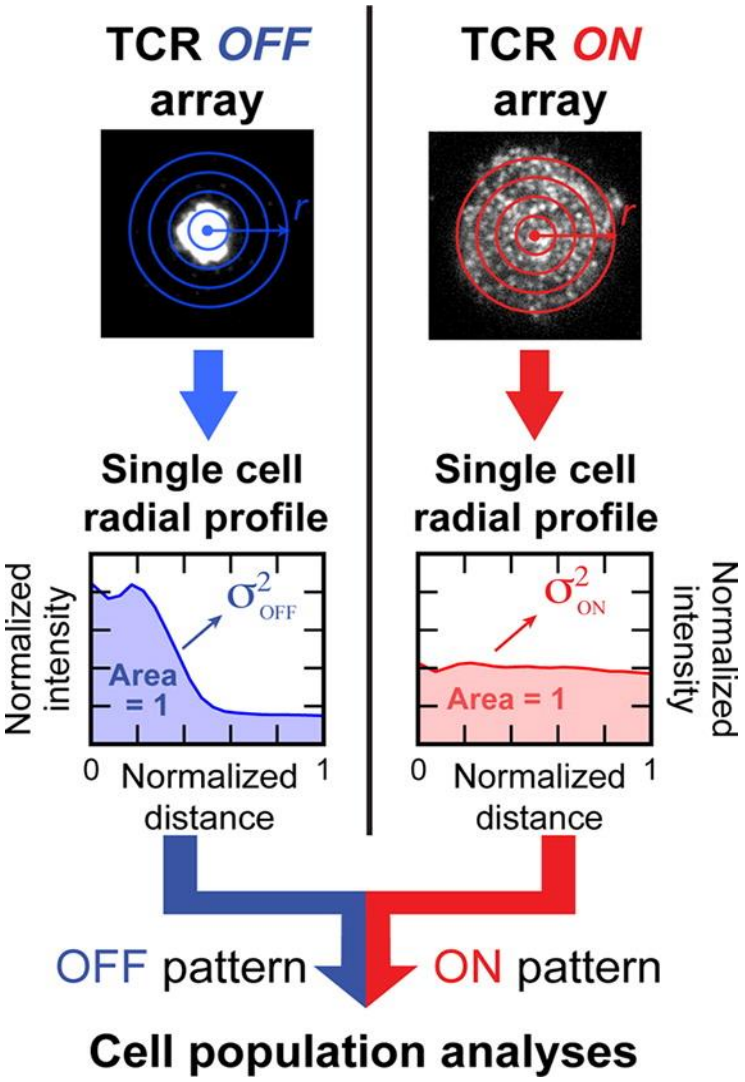


Figure 3.4. Schematic of the quantitative analysis method. Normalized radial intensity profile of the TCR image (radial probability distribution for TCR) for each cell off or on the array in the same sample. Variance of the distribution, which corresponds with the degree to which TCR transport is frustrated, was calculated for each profile generated. Population level analyses are performed thereafter.

Results from a two-dimensional titration experiment in which antigen density and nanodot array spacing are independently varied are illustrated in Figure 5. As before, the total pMHC density is fixed at 80 molecules/μm2, and the ratio of agonist to null peptide is titrated. Five different nanodot array spacings, ranging from 40 to 171 nm, as well as unpatterned membranes were examined, and a minimum of 39 cells was analyzed for each combination of conditions. Representative images with color-coded borders corresponding to population average data (see inset and Supplementary Figure S9 in the associated manuscript[19]) are depicted in matrix layout in Figure 3.5. As antigen is titrated to lower densities, the TCR clusters are able to percolate through progressively smaller nanodot arrays. Appreciable TCR transport was observed even on the 40 nm spaced arrays at agonist–null peptide ratios of 1:50 and below. These data reveal that the effective size of TCR signaling

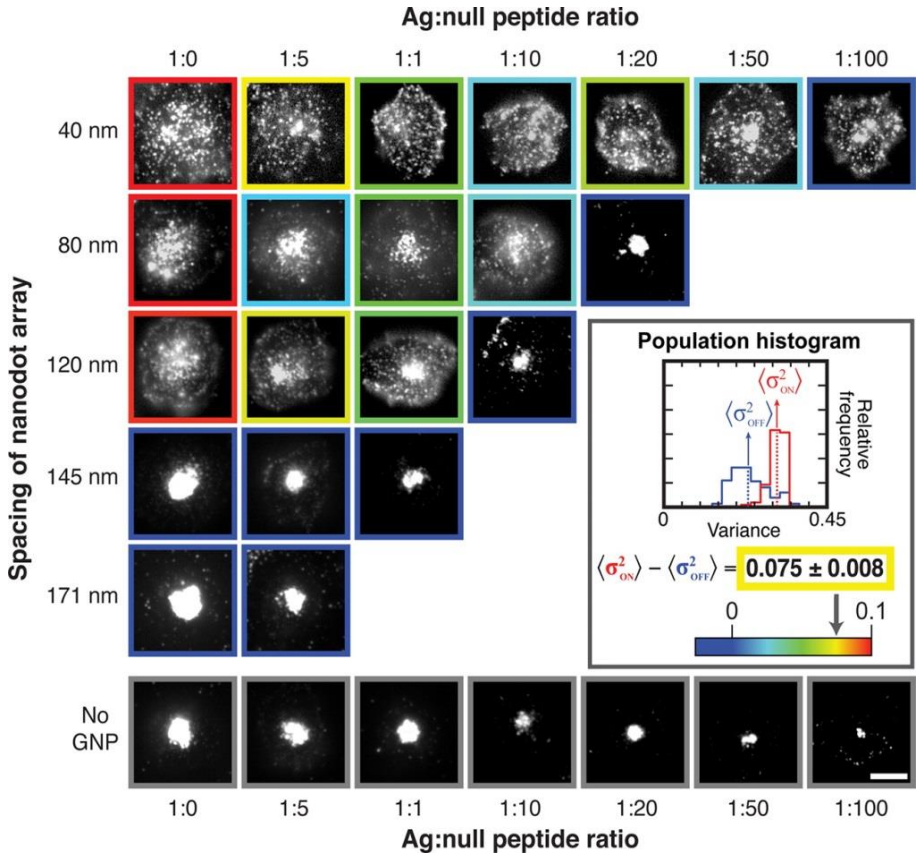


Figure 3.5. TCR microcluster chromatography with the titration of nanodot spacing and ag–null peptide ratios. Cells are fixed 20 min after contact with the SLB according to the indicated conditions, and epifluorescent images of TCR are shown. (Inset) The distribution of variance was plotted in a histogram for the cell population. The degree of TCR cluster centripetal transport is quantified as the difference between the population variance on and off the array, and the calculated value is represented as the colored borders around each TCR image.

clusters varies continuously with antigen density and that functional signaling clusters readily percolate through 40 nm spaced arrays at low antigen density.

3.4 Discussion

Structural studies of TCR and CD4 simultaneously bound to pMHC suggest that the lateral size of this complex in the T cell membrane is 10 nm in diameter.[97] Additionally, TCR–pMHC complexes require relatively close apposition of the two membranes.[94] Thus, the 10 nm high nanodots may sterically interact with other proteins associated with the TCR signaling cluster (see the scale schematic in Figure 1). As such, the physical footprint of the TCR cluster in the T cell membrane, more so than just the bound pMHC ligands in the supported membrane, is likely to define the effective cluster size as determined by percolation through the nanodot array. In support of this conclusion, we note observations of distinctly different behavior in a juxtacrine signaling system (ephrinA1–EphA2) that has a larger intercellular spacing (21 nm,[98] Supplementary Figure S10 in the associated manuscript[19]). In a hybrid live cell supported membrane junction, ephrinA1–EphA2 form signaling clusters that exhibit lateral transport in a manner reminiscent of TCR signaling clusters.[20,82,99] However,

transport of EphA2 clusters is not impeded by the nanodot array, even when the clusters are visibly larger than the array spacing.[20] The EphA2 clusters appear to be able to pass over the nanodot array. Only when some of the ephrinA1 ligand is directly affixed to the gold nanodots is any impedance imposed on the EphA2 clusters.

If TCR complexes within a cluster are assumed to pack in a rough lattice with a 10 nm unit cell, a cluster with 10 TCR would have a diameter of 30 nm and might therefore be expected to percolate through the array. The useable space between nanoparticles in the array is less than the interparticle spacing (e.g., 30 nm for the 40 nm array, accounting for the nanoparticle size itself). Nanodot array chromatography does not necessarily provide a direct caliper for the size of the TCR cluster since other properties, such as the dynamics of the TCR cluster, are naturally convolved with the percolation measurement. Nevertheless, this type of ambiguity is inherent to essentially all forms of size chromatography without significantly reducing their utility.

Collective consideration of results from the experiments described here reveals the physical nature of the TCR signaling cluster to be distinctly dependent on the amount of antigen encountered by the cell. At high antigen densities, they reach sizes that exhibit difficulty percolating through supported membrane-embedded nanodot arrays with interparticle spacings as large as 120 nm. At lower antigen densities, but still well above the threshold for triggering intracellular Ca2+ flux, TCR clusters can move through nanodot arrays with interparticle spacings as small as 30 nm. At these lower antigen densities, TCR clusters appear to be small (<10 TCR), flexible, or dynamic. This observation necessitates a reconsideration of the concept of a TCR signaling cluster to account for such antigen-dependent variability. Downstream signaling reactions within the TCR cluster must either be independent of these physical properties or perhaps regulated by them. The supported membrane-embedded nanodot array platform provides a physical means to both probe and manipulate membrane assemblies, such as the TCR signaling cluster, while they are functioning in the membrane of a living cell.

Chapter 4

Myosin IIA modulates T cell receptor transport and CasL phosphorylation during early immunological synapse formation

*The work presented in this chapter has been previously published as part of the following paper: Yu, Y., Fay, N.C., Smoligovets, A.A., Wu, H.-J., and Groves, J.T. Myosin IIA Modulates T Cell Receptor Transport and CasL Phosphorylation During Early Immunological Synapse Formation. *PLoS ONE*, 7(2):e30704 (2012).

*Yan Yu conceived and performed the experiments, analyzed and interpreted data, and wrote the manuscript. Nicole Fay performed calcium imaging experiments, analyzed and interpreted the data, prepared materials and reagents, cultured cells, and performed additional unpublished control experiments. Alexander Smoligovets made a plasmid. Hung-Jen Wu wrote Matlab scripts for data analysis.

4.1 Introduction

The spatial organization of cell membrane receptors at intercellular junctions is emerging as an important aspect of many signal transduction processes[67,82,100–102]. One paradigmatic example is T cell activation in which T cell receptors (TCRs) engage their ligands, antigenic peptide loaded major histocompatibility complex proteins (pMHC), on the surface of antigen-presenting cells (APCs). This cell-cell junction, known as the immunological synapse (IS), exhibits an elaborately choreographed spatial reorganization of proteins on multiple length scales, ranging from molecular dimensions to the size of the cell itself[7,83]. Upon the triggering, T cell receptors (TCRs) collectively nucleate into microclusters of tens to hundreds of molecules together with kinases and adaptor proteins. The signaling clusters are subsequently transported centripetally, ultimately accumulating in the central supramolecular activating complex (cSMAC) where signaling is attenuated[55,74,96,103]. Meanwhile, integrins reorganize into a ring structure, forming the peripheral supramolecular activating complex (pSMAC). Interference with protein pattern formation by physically imposed barriers to TCR translocation leads to changes in TCR phosphorylation, duration and magnitude of calcium response, as well as changes in T cell triggering thresholds[2,9,104].

In the terminology of thermodynamics, force is the conjugate variable to space. As such, spatial organization and mechanical forces are intrinsically coupled; in general, one doesn't occur without the other. In the case of the immunological synapse, forces have been implicated in its formation since its initial identification[105]. Retrograde flow of the actin cytoskeleton drives segregation of signaling complexes at the IS and is required for sustaining TCR signaling[46,48,62,106–108]. Dynein has also been shown in a recent study to drive microtubule-dependent transport of TCRs and to negatively regulate T cell signaling[109]. In the immunological synapse, the role of non-muscle myosin IIA, the myosin II isoform that is dominantly expressed in T cells, has been debated in several studies[105,110,111], but without consensus.

Here we examine the role of myosin IIA in the formation of the immunological synapse by tracking movements of TCRs, actin, and myosin with high spatial and temporal resolution. Primary T cells are activated by pMHC and inter-cellular adhesion molecule (ICAM) −1, both of which are tethered to supported lipid bilayers by polyhistidine/nickel-chelating lipid linkages. Both proteins, freely mobile in the supported bilayer, readily assemble into microclusters and larger scale organization in response to driving forces applied by the cell. This hybrid live cell – supported membrane junction enables high resolution imaging of the immunological synapse using total internal reflection fluorescence (TIRF) microscopy[112]. By analyzing movements of TCRs, actin, and myosin, we demonstrate that myosin IIA makes a distinctive contribution to TCR cluster movement during the first one to two minutes after T cell stimulation. Inhibition with blebbistatin or ML-7 reduces both calcium influx and spatial colocalization of active ZAP-70 with TCR microclusters. Thus myosin IIA contributes, at least indirectly, to TCR signaling. A more telling observation is that myosin inhibition also reduces phosphorylation of the mechanosensing protein CasL (Crk-associated substrate of the lymphocyte type), raising the hypothesis of a direct mechanical mechanism of signal modulation involving CasL.

4.2 Materials and methods

4.2.1 Animals

AND X B10.BR transgenic mice (Jackson Laboratory), of both genders and of age between 6–16 weeks, were used as CD4+ cell donors. Mice were housed in a facility certified by AWRC, under continuous veterinary animal care with adequate water, food and comfort. Only AWRC veterinary certified researchers, who have passed specific animal handling tests for the procedure, were allowed to handle the mice.

4.2.2 CD4+ cell harvest

The procedure was performed in accordance with the American Veterinary Medical Association (AVMA) Guidelines on Euthanasia. Mice were first euthanized with carbon dioxide. Cervical dislocation was performed at least 5 minutes after euthanasia to minimize pain to the mice. Mice were sterilized with 70% ethanol prior to the harvest of lymph nodes and spleen. AND CD4+ T cells were expanded to T cell blasts after harvest and maintained as previously described[9,113].

4.2.3 DNA constructs

A plasmid containing enhanced green fluorescent protein fused to the calponin homology domain of utrophin (EGFP-UtrCH)[114] was a gift of Dr. William Bement, University of Wisconsin, Madison, WI. The EGFP-UtrCH coding sequence was amplified using PCR and subcloned into a murine stem cell virus plasmid (pMSCV-Puro). A plasmid containing EGFP fused to the heavy chain of human non-muscle myosin IIA (EGFP-NMHCIIA) was provided by Dr. Robert Adelstein, National Institutes of Health, Bethesda, MD through Addgene.org (Addgene plasmid 11347)[115], and the EGFP-NMHCIIA coding sequence was subcloned into pMSCV-Puro plasmid.

4.2.4 Reagents

Histidine-tagged ICAM-1 and MHC Class II I-E^K were expressed and purified as previously described[9,61]. Briefly, secreted ICAM-1 with a decahistidine tag at its C terminus (a gift of Dr. Mark Davis, Stanford University) was expressed using the baculovirus expression system in High Five cells (Invitrogen) and purified using a Ni^{2+}-NTA-agarose column (Qiagen). Secreted MHC with a hexahistidine tag at the C terminus of both α and β chains was similarly expressed and purified from S2 cells. Blebbistatin, ML-7 and jasplakinolide were purchased from EMD Chemicals. ZAP-70 (Tyr319) antibody and p130Cas (pY165) antibody were purchased from Cell Signaling.

4.2.5 Retroviral transfection

T cells were retrovirally transduced using supernatants derived from cultures of Phoenix cells as previously described[116]. Briefly, Phoenix cells were transfected with pMSCV-Puro-EGFP-UtrCH or pMSCV-Puro-EGFP-NMHCIIA immediately prior to T cell

harvest using the calcium phosphate method. The transfected Phoenix cells were cultured in T cell medium starting 24 hours after transfection and T cell harvest. Two days after transfection and T cell harvest, T cells were spun down, resuspended in supernatant collected from the Phoenix cell cultures, and spun at 2500 min^{-1} for 1 hr to encourage uptake of virus. T cells were selected in fresh medium containing 0.5 µg/ml puromycin 3 days after harvest and were allowed to recover from selection in fresh medium 5 days after harvest. They were used for imaging experiments starting from day 7 after cell culture.

4.2.6 Bilayer assembly and cell imaging

Moth cytochrome *c* 88–103 peptide (MCC, ANERADLIAYLKQATK) (Biosynthesis and the Dana-Farber Core Facility) was loaded onto the I-E^K protein overnight. Glass-supported lipid bilayers comprised of 98 mol% 1,2-dioleoyl-sn-glycero-3-phosphocholine (DOPC) and 2 mol% 1,2-dioleoyl-sn-glycero-3-[(N-(5-amino-1-carboxypentyl)iminodiacetic acid) succinyl] (nickel salt) (Ni^{2+}-NTA-DOGS) (Avanti Lipids) were prepared in flow chambers by standard methods[2,9,48]. Bilayers were loaded with ICAM-1 and pMHC by incubation at room temperature for 40 minutes. To label the T cell receptors, the non-blocking antibody H57 αTCR-Fab (conjugated to Alexa Fluor 594 or Alexa Fluor 643 as indicated) was incubated with T cells at 4°C for 20 min. To inhibit myosin or actin depolymerization, cells were then incubated with 100 µM blebbistatin, 20 µM ML-7 or 1 µM jasplakinolide at 37°C for 15 min before imaging. Inhibitors used at the indicated concentrations have been shown to effectively inhibit functions of their target proteins[117–119]. For fixed cell experiments, cells were injected into a sample chamber preheated to 37°C and allowed to interact with the bilayer for the indicated time. Cells were then fixed with 2% paraformaldehyde, permeabilized with 0.05% Triton X, blocked with 5% casein and labeled with antibodies at room temperature or as otherwise indicated. To label pZAP-70, fixed cells were incubated with anti-pZAP-70 IgG against Tyr319 (Cell Signaling) at 4°C overnight and then with Alexa Fluor-488 conjugated goat anti-rabbit IgG (Invitrogen) at room temperature for 20 min. Because the YxxP motifs are highly conserved between CasL and p130Cas, the YxxP motifs of CasL were labeled with p130Cas (pY165) antibody (Cell Signaling). Total internal reflection fluorescence (TIRF) microscopy images were acquired on a Nikon Ti-E/B inverted microscope with a 100× 1.49 NA oil immersion TIRF objective and an Andor iXon EMCCD camera. Images of phosphorylated pZAP70 or pCasL of different samples were acquired under the exact same settings for lasers, camera, and microscope; the angle of the input laser was also kept consistent throughout imaging under the control of a motorized laser TIRF illumination unit (Nikon) and the focus on the glass substrate was maintained by a Perfect Focus System (Nikon).

4.2.7 Calcium imaging

T cells were firstly incubated with 1 µM Fura-2-acetoxymethyl ester (Fura-2 AM) in serum-free cell media at room temperature for 15 minutes and then in Fura-2 free serum-rich media at 37°C for 20 minutes. After TCR labeling, cells were incubated with DMSO or 20 µM ML-7 at 37°C for 15 min before being injected into the imaging

chamber. Images were acquired on a Nikon TE 2000 microscope with a 40× S Fluor objective (Nikon) and a Coolsnap K4 camera (Roper Scientific). Emission at 510 nm was captured by alternating the excitation wavelength between 340 and 380 nm. The ratiometric value of the Fura-2 AM dye, indicating relative intracellular calcium levels, was obtained by using the program Imaris (Bitplane) and a custom Matlab algorithm.

4.2.8 Speckle tracking and image analysis

The custom speckle tracking algorithm as described previously[46,107], was used to identify the locations of speckles based on the fluorescent intensity gradient within the images. Following identification, nearest neighbors of speckles in consecutive frames were linked to generate trajectories. The position- and time- averaged radial velocities of the speckles relative to the defined cell center were then analyzed. Time-averaged radial velocity $<V(t)>$ was obtained by averaging the radial velocities of all microclusters located at the cell periphery during $(t, t+\Delta t)$, where t is the elapsed time after the initial cell-bilayer contact and Δt = 10 sec. The object-based colocalization algorithm contains two major steps: cluster identification and pairwise cluster matching between two fluorescent channels. The fluorescent clusters were firstly identified by the speckle tracking algorithm. The microclusters in two fluorescent channels are considered as colocalized if their center distance is within the diffraction limit (200 nm). TCRs accumulated in the cSMAC area were excluded from the analysis for control cells at 5 min due to their distinct signaling properties and the absence of ZAP-70 in this region[96]. The cSMAC region was outlined based on the higher fluorescence intensity by applying an imaging threshold calculated from Otsu's algorithm[120]. For the direct comparison of the phosphorylation level of pZAP-70 or pCasL between different samples, analysis was done in multiple steps. (1) Cells were first selected manually and outlined in each image. (2) Fluorescence intensities of all pixels at each cell-bilayer contact area were summed and an averaged fluorescence intensity per cell (I_{ave}) subtracted by background was obtained. (3) I_{ave} of each sample was then normalized to that of the control.

4.3 Results

4.3.1 Myosin IIA transiently drives translocation of TCR microclusters

During antigen recognition, TCR-pMHC complexes undergo a series of spatial translocations including: local clustering and long range transport to the center of the IS[7,74,83,96,103]. To explore the role of myosin IIA in these steps, we imaged fluorescently labeled TCRs at the cell-bilayer interface and tracked their movements with a custom tracking algorithm that implements an intensity gradient method to find centers of non-spherical fluorescent objects. Essentially, the entire ensemble of TCR microclusters within each individual cell (~100 microclusters) was imaged and tracked with ~50 nm spatial resolution and ~50 ms temporal resolution over the course of IS formation. In control cells, TCR trajectories reveal coordinated centripetal movement in pSMAC region and the cell periphery following the initial cell-bilayer contact, but more confined motion at the center (cSMAC) (Figure 4.1A). Pharmacological inhibition of myosin IIA by

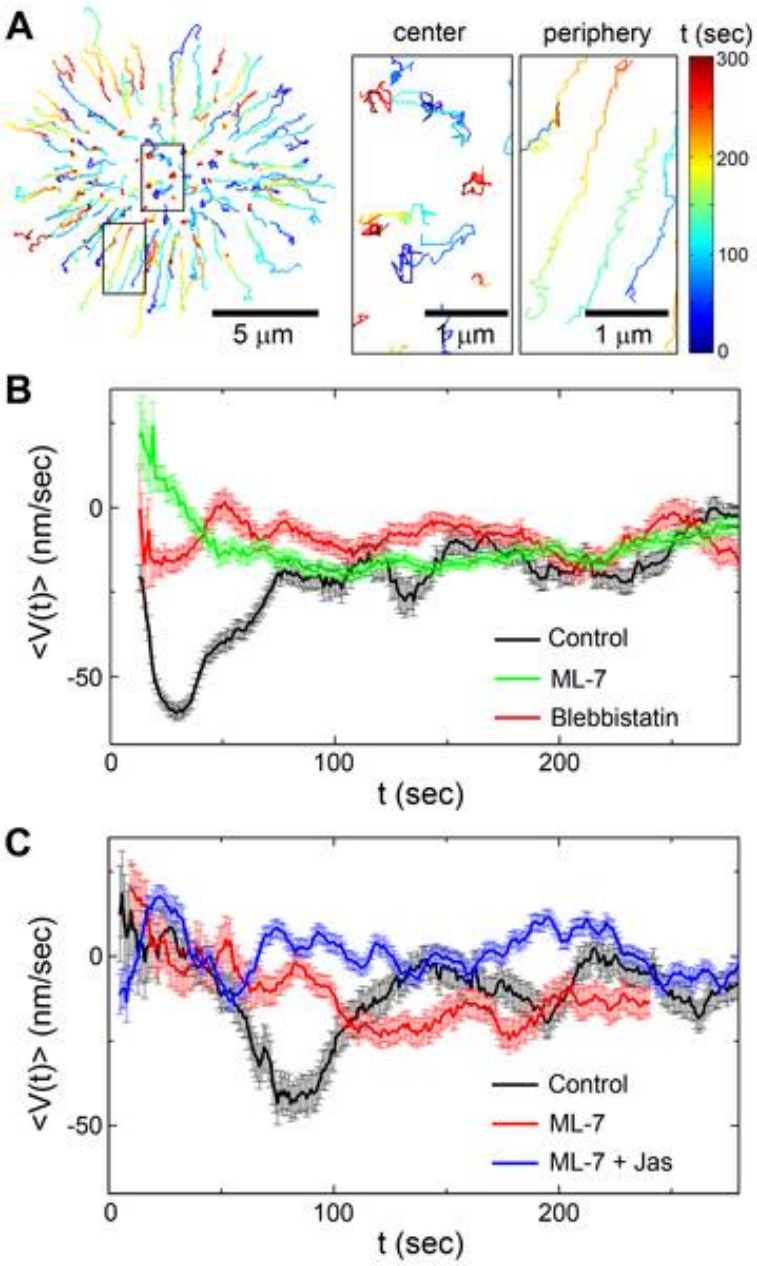


Figure 4.1. Myosin IIA transiently drives TCR translocation and actin retrograde flow in immunological synapse formation. T cell receptors (TCRs) were labeled with H57 αTCR Fab (Alexa Fluor dyes) and imaged starting from the initial cell-bilayer contact (t = 0 sec). (**A**) Trajectories of all TCR microclusters (Alexa Fluor 594) show their centripetal movement at the cell periphery and highly confined motion at the central area of the immunological synapse. Color bar corresponds to the elapsed time after the initial cell-bilayer contact. Data are representative of 6 independent experiments. (**B**) Inhibition of myosin IIA changes the time-dependence of TCR microcluster translocation. Time-averaged radial velocities (<V(t)>) of TCRs (Alexa Fluor 643) in individual cells are plotted against the elapsed time after the initial cell-bilayer contact in the presence of DMSO control, blebbistatin, or ML-7. Data are representative of 5 independent experiments. (**C**) Inhibition of myosin IIA changes the time-dependence of actin retrograde flow during the immunological synapse formation. Time-averaged radial velocities (<V(t)>) of tracked EGFP-UtrCH in individual cells are plotted against the elapsed time after the initial cell-bilayer contact in the presence of DMSO control, ML-7, or ML7 with jasplakinolide. Data are representative of 4 independent experiments. Error bars in (**B**) and (**C**) represent standard errors.

blebbistatin (100 μM) and ML-7 (20 μM) does not alter the clustering of TCRs, but leads to much less directed motion of the microclusters (Figure S1 in the associated manuscript[86]). For a more quantitative measure, we analyzed the time-dependence of TCR translocation during IS formation. Averaged radial velocities, <V(t)>, are plotted against time, t, on a single cell basis. <V(t)> is defined negative for centripetal movements and positive for movements toward the cell periphery. In control cells, translocation of TCR microclusters varies significantly as IS formation proceeds (Figure 4.1B). After the initial cell-bilayer contact (t = 0 sec) microclusters undergo very rapid centripetal movement ($\langle V(t)\rangle_{max} \approx -70$ nm/sec) for approximately 2 min and then

maintain a reduced yet constant speed (<V(*t*)>≈−15 nm/sec) for an additional 3–5 min until the central accumulation of TCRs stabilizes. By contrast, TCR microclusters in cells pretreated with blebbistatin or ML-7 do not exhibit the rapid initial centripetal movement, but move at an almost constant velocity (<V(*t*)>≈−10 to −15 nm/sec) throughout the entire time course of IS formation (Figure 4.1B). The loss of the initial rapid component of centripetal movement indicates that myosin IIA is transiently involved in TCR transport and the slower movement in the presence of myosin inhibitors suggests a secondary driving force, presumably actin polymerization. In control experiments in which we simultaneously imaged TCR translocation and cell edge movement, we confirm that TCR microclusters, which move almost one order of magnitude faster than the cell membrane contraction (−5 nm/sec), are actively driven by forces from myosin IIA instead of the global cell movement (Figure S2 in the associated manuscript[86]).

Next, we quantified the effect of myosin IIA on actin retrograde flow during IS formation by imaging and tracking actin labeled with the calponin homology domain of utrophin fused to EGFP (EGFP-UtrCH)[46,114]. Myosin IIA is known to exert contractile forces on the actin cytoskeleton for various cellular functions[121–124]. In agreement with previous reports[106], the flow of actin in control cells shows the same time-dependence as that of TCR microclusters: a rapid centripetal flow followed by a persistent and slower flow (Figure 4.1C and Figure S3 in the associated manuscript[86]). Similar to the effect of myosin inhibition on TCR translocation, actin flow in cells pretreated with ML-7 exhibits only a constant velocity of ≈−10 nm/sec. Blebbistatin was not used here due to its photoinactivation by short wavelength light[125]. Results from both TCR movement and actin flow indicate that myosin IIA transiently contributes to actin retrograde flow and, correspondingly, TCR transport during early times of IS formation. In T cells treated with both ML-7 (20 μM) and jasplakinolide (1 μM), a pharmacological agent to prevent actin depolymerization, actin retrograde flow is completely abrogated (Figure 4.1C). Therefore, actin polymerization provides a long-lasting driving force that operates in superposition to the more transient contribution from myosin.

The role of myosin IIA in IS formation has been controversial in previous studies[105,110,111]. Since our fluorescence tracking data suggests that TCR microclusters are able to translocate in the absence of myosin IIA, we studied whether myosin is required for the spatial organization at the IS. TCR and ICAM-1 in control cells exhibit the characteristic “bull's eye” pattern, where the TCR microclusters accumulate at the center while LFA-1 bound to ICAM-1 localizes at the periphery (Figure 4.2). Inhibition of myosin leads to a more dispersed distribution of TCR microclusters in cells fixed at 3 min after stimulation, but the difference becomes negligible when cells are fixed at 10 min (Figure 4.2 and Figure S4 in the associated manuscript[86]). The overall ring-like distribution of ICAM-1 in the pSMAC is not affected by myosin inhibition. This demonstrates that myosin IIA influences the time frame of IS formation, but is not required for the superficial appearance of the final pattern. It is important to recognize that these observations do not suggest that the cells arrive at the same final state with and without myosin, as detailed below. Rather, it reveals that the large scale spatial organization of the IS probably offers insufficient information from which to judge the more subtle internal state of the cell.

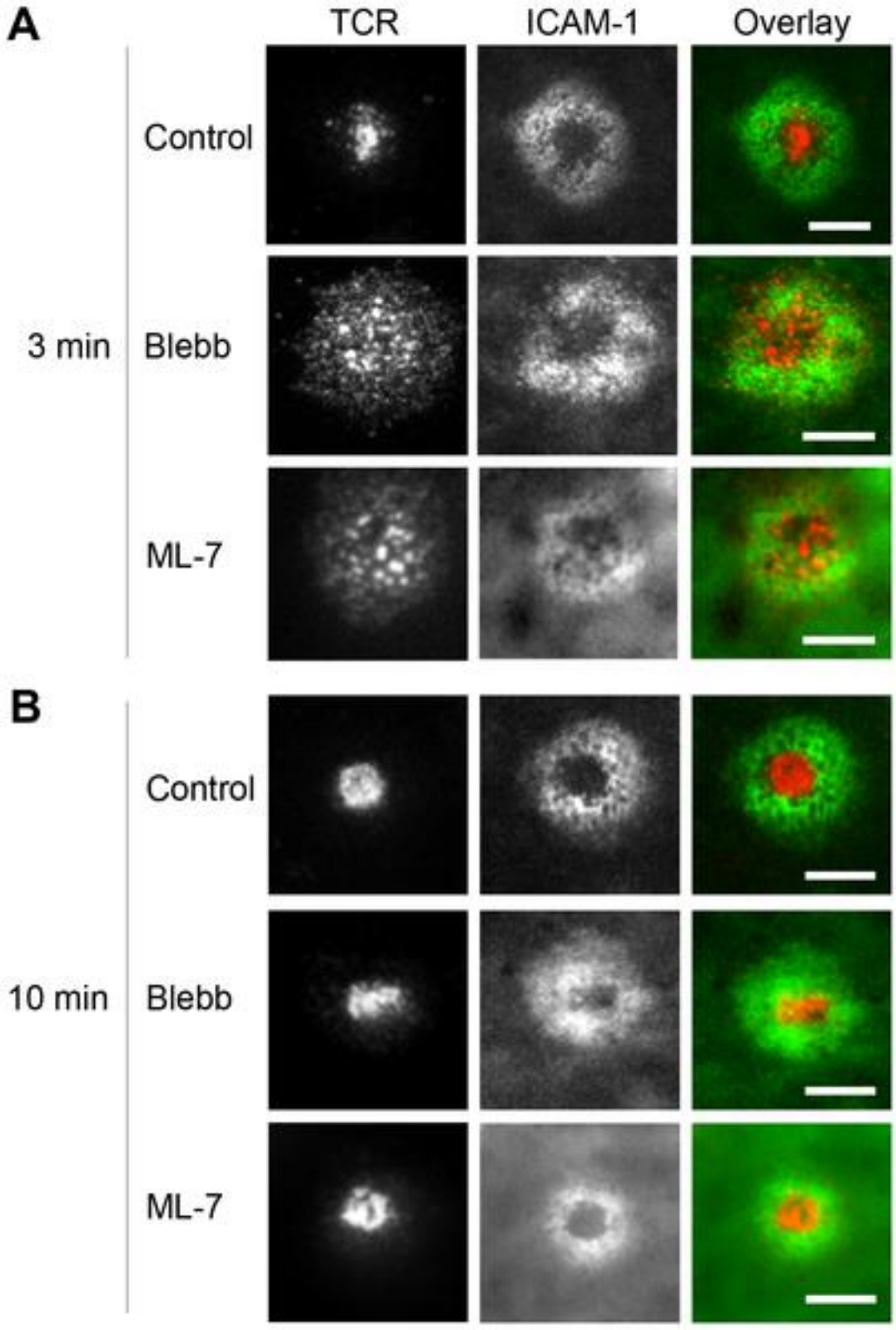


Figure 4.2. Inhibition of myosin only affects morphology of the early immunological synapse. Total internal reflection fluorescence (TIRF) images of TCRs labeled with H57 αTCR Fab (Alexa Fluor 594) and ICAM-1 (Alexa Fluor 488) are shown. Cells were pretreated with DMSO, blebbistatin, or ML-7, and fixed at (**A**) 3 min and (**B**) 10 min after interacting with bilayers. Data are representative of 3 independent experiments. Scale bars: 5 μm.

4.3.2 Forces applied to TCR clusters are translated to myosin IIA

Our results above have shown that myosin IIA transports TCR microclusters by driving actin retrograde flow. To further explore the mechanical link between myosin and TCR, we quantified if physical forces on TCR clusters can be transmitted to influence myosin. We formed lipid bilayers on substrates patterned with metal grids, which create barriers to lateral mobility of membrane-tethered pMHC and ICAM-1. Because patterned bilayers retain their fluidity[9,17,46,62,107], TCRs engaged with the constrained pMHC are trapped by the metal grids and experience passive opposing forces from the barriers that prevent their centripetal movement. As shown in Figure 4.3A, the adhesion of T cells and local clustering of TCRs remain unchanged on the patterned lipid bilayers, but TCR centripetal translocation is blocked by the metal barriers. The question, then, is how this physical trapping of TCR clusters affects myosin, which is itself not directly influenced by the substrate-imposed patterns. By plotting the radial velocity (<V(*t*)>)

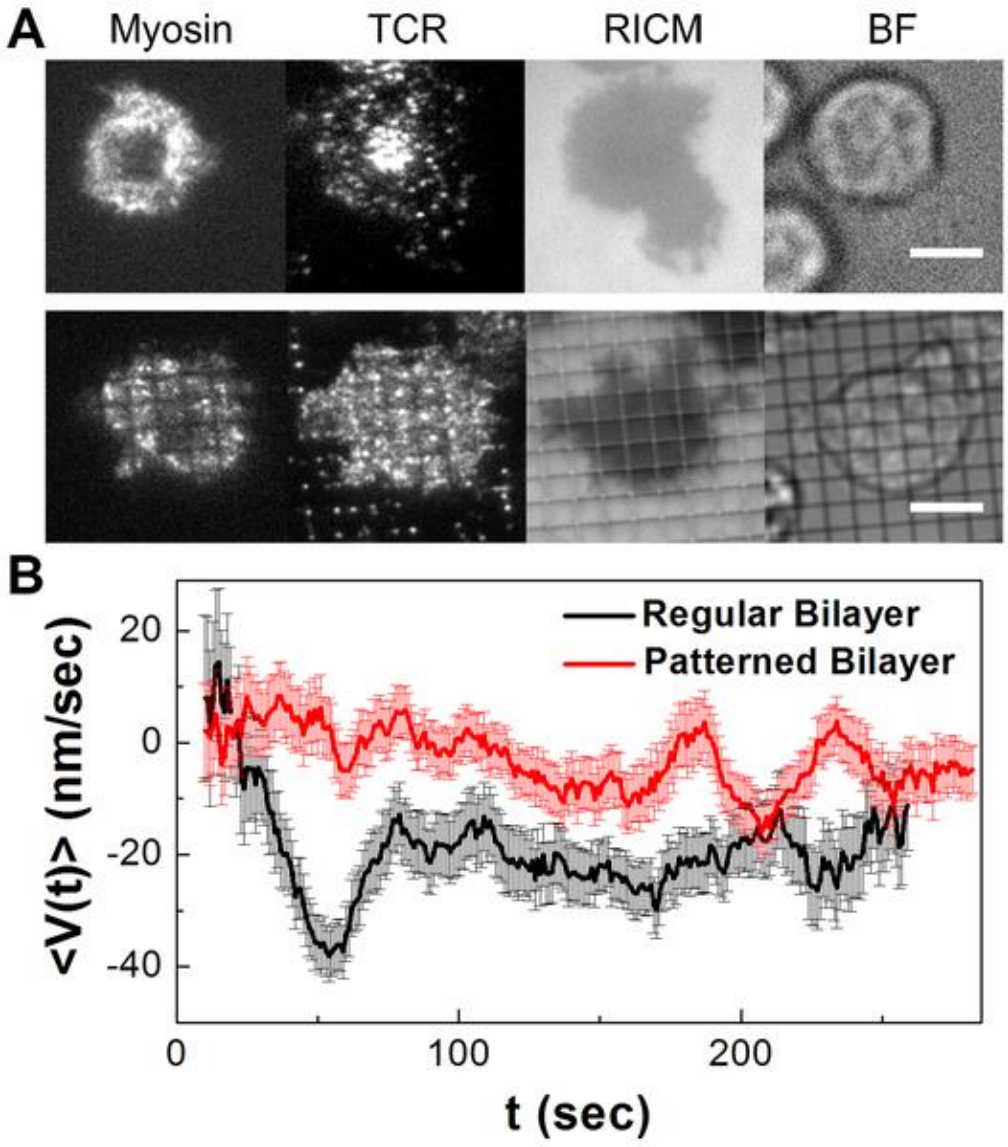


Figure 4.3. Physical constraints on TCR microcluster translocation impede myosin IIA movements. (**A**) TIRF, reflection interference contrast microscopy (RICM), and bright field (BF) images of T cells expressing EGFP-myosin on unpatterned or patterned bilayers. Scale bars: 5 μm. (**B**) Time-averaged radial velocities (<V(*t*)>) of EGFP-myosin in individual cells are plotted against the elapsed time (*t*) after the initial cell-bilayer contact (*t* = 0). Data are representative of 2 independent experiments.

against time (*t*), we observed that myosin exhibits similar time-dependent motion as that of TCR and actin on non-patterned lipid bilayers. However, on a patterned bilayer where TCR microclusters are hindered from moving past the metal line grids, the centripetal movement of myosin IIA at earlier times is significantly reduced (Figure 4.3B). By performing the same experiments on actin, we also observed that actin retrograde flow decreases on the patterned lipid bilayers consistently with myosin (Figure S5 in the associated manuscript[86]). The slow-down of myosin in response to physically constrained TCRs confirms the existence of a mechanical coupling between TCR and myosin. Moreover, because contractile forces in actin are generated by myosin and studies have shown that resistive load on non-muscle myosin IIA leads to its slower power stokes on actin[126], the reduced actin retrograde flow on pattern lipid bilayers points to actin cytoskeleton as responsible for transmitting the resisting force from TCR microclusters to myosin.

4.3.3 Myosin IIA is required for Ca^{2+} influx

A hallmark of T cell activation downstream of TCR signaling is the elevation of

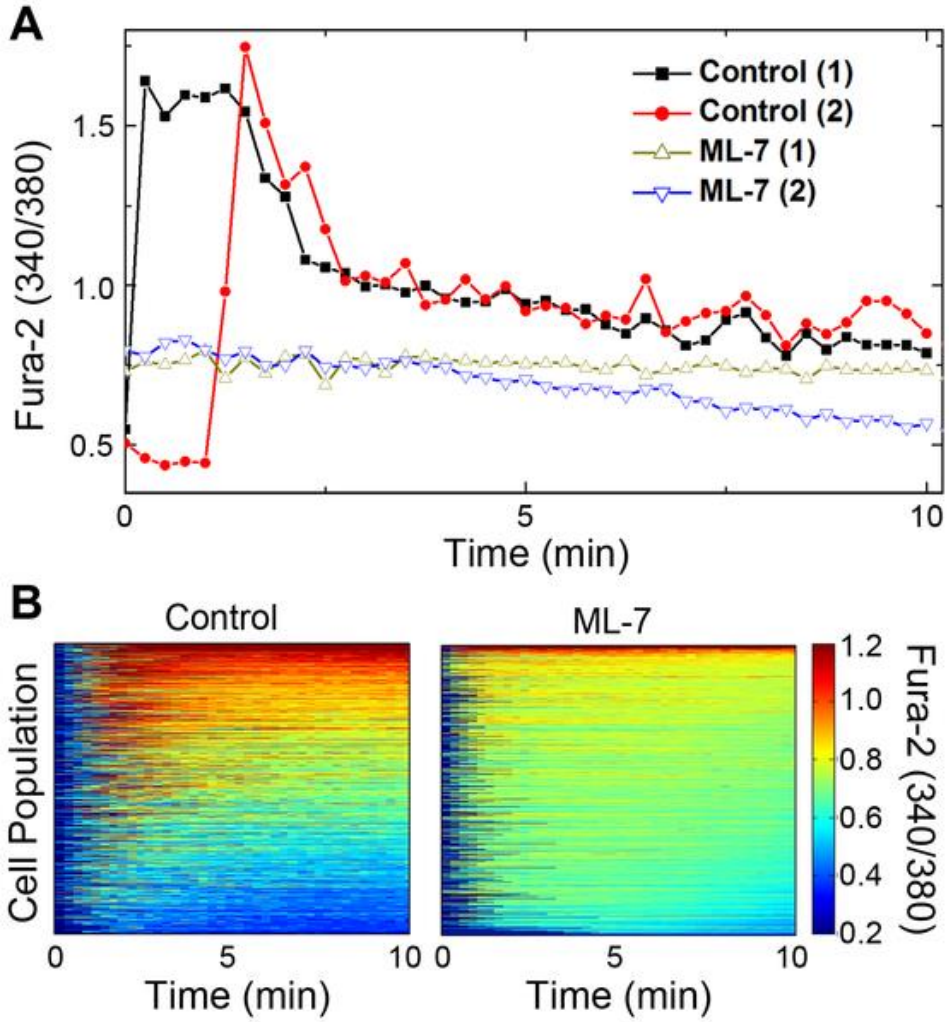


Figure 4.4. Inhibition of myosin IIA abolishes intracellular Ca^{2+} influx. The ratio of Fura-2 fluorescence emission intensity in response to 340 nm and 380 nm excitation (340/380) is proportional to intracellular [Ca^{2+}]. (**A**) Fura-2 340/380 emission ratios are plotted against the cell stimulation time for four representative cells pretreated with either DMSO or ML-7. (**B**) Fura-2 340/380 emission ratios of control cells (n = 1602) and cells pretreated with ML-7 (n = 2187) are plotted against time on a color scale and organized along the *y*-axis according to the summed calcium influx.

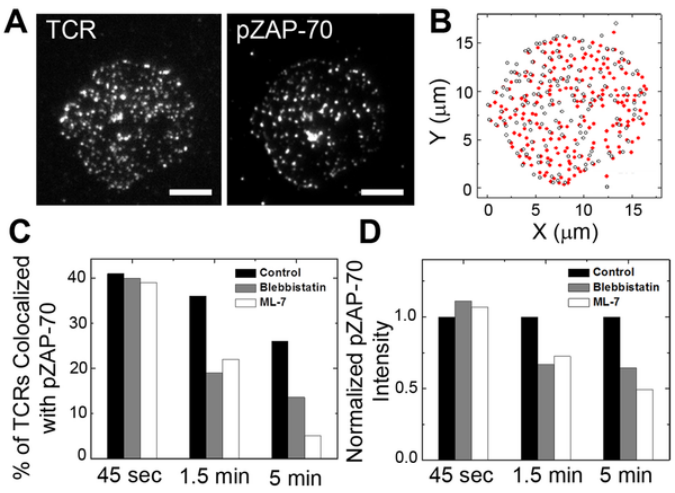


Figure 4.5. Inhibition of myosin IIA reduces phosphorylation of ZAP-70 and colocalization of pZAP-70 with TCR microclusters. (**A**) TIRF images of TCR and pZAP-70 (pY319) from a T cell fixed at 1.5 min. (**B**) Object-based colocalization analysis identifies TCRs and pZAP-70 in the T cell in panel (**A**). (**C**) The percentages of TCR microclusters colocalized with pZAP-70 are shown for the indicated stimulation times prior to fixation. (**D**) Fluorescence intensities of pZAP-70 in IS are shown normalized to those in control cells. Each column in panel (**C**) and (**D**) is an averaged value from approximately 200–300 cells. Data were reproduced in 2 independent experiments. Scale bars: 5 μm.

intracellular calcium, which in turn activates a number of calcium-dependent pathways[127]. We used Fura-2 as the indicator of intracellular calcium concentration; the ratio of its emission intensities at 340 nm excitation versus 380 nm is proportional to Ca^{2+} concentration. In control cells, intracellular Ca^{2+} concentration rapidly increases within 1 min after the initial cell-bilayer contact. By contrast, cells pretreated with ML-7 do not show any significant Ca^{2+} elevation, but maintain a low Ca^{2+} level similar to baseline (Figure 4.4A). The Ca^{2+} concentration traces of a large population of both control cells and cells pretreated with ML-7 show a dramatic reduction in the calcium influx in response to myosin IIA inhibition (Figure 4.4B). In agreement with previous work on Jurkat cells[111], the results show that myosin IIA is important for calcium signaling in primary T cells.

4.3.4 Inhibition of myosin IIA reduces association of active ZAP-70 with TCR

T cell signaling is initiated in discrete TCR microclusters, and association of kinases and adaptor proteins with the microclusters is a key step of sustaining the signaling reaction[74,96,127–129]. Upon TCR engagement to pMHC, ZAP-70 is recruited to the CD3 zeta chain and phosphorylated on tyrosine 319 (pZAP-70) for downstream signaling. To understand the role of myosin IIA in initiation of TCR signaling, we used ZAP-70 as a quantitative readout of TCR/CD3 signaling and quantified how myosin inhibition influences colocalization of pZAP-70 with TCR using an object-based colocalization algorithm. Unlike many intensity-based colocalization algorithms[130], this analysis avoids bias due to the variation in fluorescence intensities between TCR microclusters (Figure 4.5B). In control cells, pZAP-70 localizes mainly on the cell periphery and its colocalization with TCR decreases with stimulation time (Figure 4.5A and C, Figure S6 in the associated manuscript[86]). Inhibition of myosin IIA results in less colocalization of TCR microclusters with pZAP-70 in T cells fixed at both 1.5 min and 5 min after stimulation, but not at 45 sec (Figure 4.5C). The phosphorylation level of ZAP-70 at the IS also decreases in the absence of myosin function (Figure 4.5D). Myosin IIA therefore contributes to the stable association of active ZAP-70 with TCR, but it is not necessary for the initial recruitment.

4.3.5 Inhibition of myosin IIA reduces CasL phosphorylation

To our knowledge, there have been no previous studies directly quantifying the cytoskeletal strain in T cells and correlating this to TCR signaling. The data we report above and other published results clearly indicate at least an indirect influence of myosin IIA on TCR signaling, but the role of its mechanical forces in the process still remains unclear. To explore that question we studied the phosphorylation of CasL. It is a member of the mechanosensing Cas protein family and is predominately expressed in T lymphocytes[131–134]. All Cas family proteins contain a highly conserved Src kinase substrate domain, which is consisted of multiple Tyr-x-x-Pro (YxxP) motifs. Studies on p130Cas, one of the Cas proteins, have shown that mechanical stretching changes conformation of the motifs and leads to enhancement of tyrosine phosphorylation and possibly downstream signaling[135]. Whether or not CasL is involved in molecular force transduction is less clear, but its phosphorylation level strongly depends on actin integrity in several cell types[136–138], suggesting that CasL might also function as a mechanosensor. Therefore, we investigated if CasL plays a possible role to transduce myosin contractile forces to modulate TCR signaling.

We quantified the phosphorylation of CasL by using a phosphorylation-specific antibody against its YxxP motifs and measuring the fluorescence intensity of secondary antibodies at the IS. It has been previously reported that either TCR or integrin crosslinking leads to CasL phosphorylation through possibly independent signaling pathways, and that the phosphorylation level upon TCR ligation peaks transiently within the first 5 min after stimulation while integrin crosslinking results in a later but more long-lasting phosphorylation[131]. Because our entire study here focuses on the early events of T cell signaling as well as the relevance between TCR and myosin, only pMHC was present in the supported lipid bilayer to exclude the potential influence of integrin signaling pathways on CasL function. While the nature of the IS is somewhat

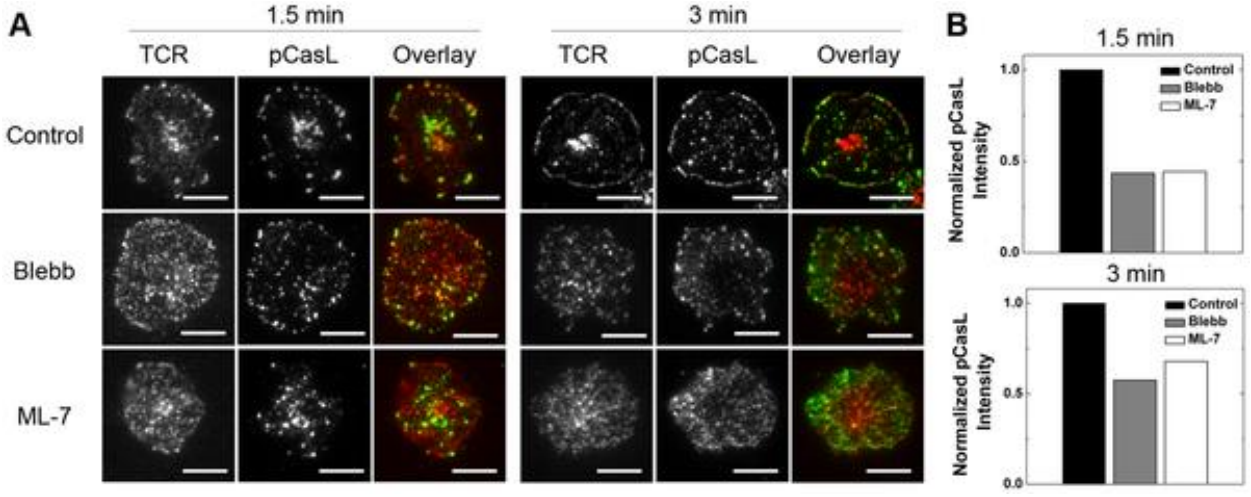


Figure 4.6. Inhibition of myosin IIA reduces phosphorylation of CasL. (**A**) TIRF images of TCR and pCasL from T cells fixed at 1.5 min and 3 min and pretreated with DMSO (control), blebbistatin or ML-7. (**B**) Fluorescence intensities of pCasL in IS are shown normalized to those in control cells. Each column in Panel (**A**) and (**B**) is an averaged value from approximately 200 cells. Data were reproduced in 2 independent experiments. Scale bars: 5 μm.

different without ICAM-LFA interactions, T cells can adhere and be normally activated by bilayer-tethered pMHC alone[1]. As shown in Figure 5.6A, phosphorylated CasL (pCasL) in control cells colocalizes with TCR microclusters across the entire IS at 1.5 min after stimulation. However, at a later time point (t = 3 min), pCasL is absent from the cSMAC region but still colocalizes with the discrete TCR microclusters on the cell periphery. Inhibition of myosin IIA has negligible effects on colocalization of TCR microclusters with pCasL, quantified by using the object-based colocalization analysis (Figure S7 in the associated manuscript[86]). However, immunofluorescence quantification of pCasL at the IS shows significantly reduced phosphorylation of CasL by myosin inhibition at both 1.5 min and 3 min after stimulation (Figure 5.6B).

4.4 Discussion

It is increasingly clear that the ability of cells to sense, interpret, and respond to mechanical signals plays a critical role in modulating diverse cellular functions, such as proliferation, migration, differentiation and homeostasis[139–142]. While integrins are the well-known force transducers in cells, recent data suggest that membrane receptors that are not directly associated with focal adhesions may also couple into force sensing roles, at least indirectly[82]. In T cells, the concept of force sensing is not well established although a number of recent studies have suggested the idea of mechanosensing in T cell activation[143–145]. We suggest that an indirect role for force in TCR signaling is all but guaranteed by the known significance of spatial organization in this system[2,9,46,48,62,104,107]. Any applied force that changes protein spatial organization in a manner to impact signaling reactions affords an indirect force response to the system. The resulted signaling, however, may be either reduced or enhanced depending on the exact mechanism. Previous studies have reported that impeded translocation of TCR microclusters leads to enhanced signaling, likely due to attenuated signal degradation at cSMAC[9,109,128]. By contrast, our results, in agreement with a previous study[111], suggest that inhibition of myosin leads to slower TCR transport and diminishes signaling. The bigger question is whether force from myosin plays a direct role in the modulation of TCR signaling. Although actin, microtubule, and some molecular motors have all been shown to play important mechanical roles in T cell signaling[74,105,106,109,111], they are unlikely to directly transduce mechanical forces into biochemical signaling cascades. Our observation of a decrease in CasL phosphorylation in response to myosin inhibition suggests that CasL may be involved in a mechanical signal transduction process in T cells. While working out details of the possible regulatory pathways is well beyond the scope of this paper, CasL is clearly a candidate for relating myosin to TCR signaling pathways. Studies have shown that CasL may be a substrate for Fyn and Lck, two key tyrosine kinases in initiating TCR activation[134]. Phosphorylated CasL can also bind to Src homology (SH) domains of signaling proteins, such as Crk, Cbl, and nucleotide exchange protein C3G, to regulate T cell signaling[146,147]. We observed the phosphorylation of CasL upon TCR ligation and its association with discrete TCR microclusters at the IS. Our results of calcium influx, ZAP-70 phosphorylation, and TCR microcluster formation all suggest that myosin is more important for sustained signaling than initiation. CasL might be involved in a feedback loop between myosin and multiple signaling pathways. While much remains to be uncovered concerning the nature of

mechanical influences on TCR activation, our observation of differential CasL phosphorylation with myosin inhibition clearly pinpoints a starting point to look into.

Chapter 5

Closing remarks

T cells employ a number of methods for fine-tuning the activation threshold. Discovering these methods of self-regulation has enabled a surge of novel therapeutics. One such example is the CTLA-4 antibody blockade that endowed T cells with the ability to recognize and clear tumor cells.[148,149] Indeed, investigations into this field have allowed the engineering of novel T cell receptors that may revolutionize personalized medicine.[150,151] Despite the great potential of immunotherapy, many basic molecular mechanisms regarding T cell signaling remain unresolved. A disastrous example of tampering with the immune system without fully understanding the overlapping, interconnected nature of the signaling networks, was with the TGN142 drug trial.[152,153] This trial, using an antibody to CD28, was expected to dampen autoimmune disorders. However, the resulting overactivation of various T cell populations resulted in multiple organ failure, lymphoma, and amputation of extremities for the six healthy volunteers.[152,153] Because of the risky nature of changing anything dictating T cell activation, novel therapeutics are being designed with “cellular kill switches” to prevent the disaster from the TGN142 trial.[154] This trial resulted in a better understanding of the human T cell repertoire, however, more research dissecting the components of this signaling network are necessary to fully harness the potential of immunotherapy.

Areas that have been left unexplored include a more detailed mechanism of T cell receptor cooperativity. Lack of TCR molecular cooperativity, in terms of stoichiometric recruitment, indicates that some other mechanism of intracellular feedback is occurring.[3] This was also observed in my dissertation chapter 1 where I demonstrated that MCC-MHC surface density altered CD80 internalization. To better resolve the mechanism of receptor cooperativity, single-molecule tracking assays using TCR and CD80 on SLBs might shed light on the feedback mechanism. Additionally, it would be useful to image immediately downstream converging molecules such as Lck, and PI3K. Calcium, while a standard for measuring T cell activation, is a ubiquitous secondary messenger and involved in many cell cycle pathways. Resolving calcium flux correlation with NFAT translocation and number of engaged MCC-MHC would reveal various steps in the signal amplification process not seen in a single live cell before. These research projects would illuminate the overlapping, cross-talk heavy T cell receptor feedback mechanisms that have confounded novel therapeutics. We would also gain insight into how such an exquisitely sensitive and specific signal transduction scheme operates.

Bibliography

1. Huppa, J. B. *et al.* TCR-peptide-MHC interactions in situ show accelerated kinetics and increased affinity. *Nature* **463,** 963–967 (2010).

2. Manz, B. N., Jackson, B. L., Petit, R. S., Dustin, M. L. & Groves, J. T-cell triggering thresholds are modulated by the number of antigen within individual T-cell receptor clusters. *Proc. Natl. Acad. Sci. U. S. A.* **108,** 9089–94 (2011).

3. O'Donoghue, G. P., Pielak, R. M., Smoligovets, A. A., Lin, J. J. & Groves, J. T. Direct single molecule measurement of TCR triggering by agonist pMHC in living primary T cells. *Elife* **2,** e00778 (2013).

4. Saline, M. *et al.* The structure of superantigen complexed with TCR and MHC reveals novel insights into superantigenic T cell activation. *Nat. Commun.* **1,** 119 (2010).

5. Pardoll, D. M. The blockade of immune checkpoints in cancer immunotherapy. *Nat. Rev. Cancer* **12,** 252–64 (2012).

6. Huse, M. The T-cell-receptor signaling network. *J. Cell Sci.* **122,** 1269–73 (2009).

7. Monks, C. R. F., Freiberg, B. A., Kupfer, H., Sciaky, N. & Kupfer, A. Three-dimensional segregation of supramolecular activation clusters in T cells. *Nature* **395,** 82–86 (1998).

8. Qi, S. Y., Groves, J. T. & Chakraborty, A. K. Synaptic pattern formation during cellular recognition. *Proc. Natl. Acad. Sci. U. S. A.* **98,** 6548–53 (2001).

9. Mossman, K. D., Campi, G., Groves, J. T. & Dustin, M. L. Altered TCR signaling from geometrically repatterned immunological synapses. *Science* **310,** 1191–3 (2005).

10. Groves, J. T. Molecular organization and signal transduction at intermembrane junctions. *Angew. Chem. Int. Ed. Engl.* **44,** 3524–38 (2005).

11. DeMond, A. L. & Groves, J. T. Interrogating the T cell synapse with patterned surfaces and photoactivated proteins. *Curr. Opin. Immunol.* **19,** 722–7 (2007).

12. Yokosuka, T. *et al.* Spatiotemporal regulation of T cell costimulation by TCR-CD28 microclusters and protein kinase C theta translocation. *Immunity* **29,** 589–601 (2008).

13. Yokosuka, T. *et al.* Spatiotemporal Basis of CTLA-4 Costimulatory Molecule-Mediated Negative Regulation of T Cell Activation. *Immunity* **33,** 326–339 (2010).

14. Yokosuka, T. & Saito, T. Dynamic regulation of T-cell costimulation through TCR-CD28 microclusters. *Immunol. Rev.* **229,** 27–40 (2009).

15. Choudhuri, K. *et al.* Polarized release of T-cell-receptor-enriched microvesicles at the immunological synapse. *Nature* **advance on,** (2014).

16. Varma, R., Campi, G., Yokosuka, T., Saito, T. & Dustin, M. L. T cell receptor-proximal signals are sustained in peripheral microclusters and terminated in the central supramolecular activation cluster. *Immunity* **25,** 117–27 (2006).

17. Groves, J. T. T., Ulman, N. & Boxer, S. G. Micropatterning Fluid Lipid Bilayers on Solid Supports. *Science (80-.).* **275,** 651–653 (1997).

18. Lohmüller, T. *et al.* Supported membranes embedded with fixed arrays of gold nanoparticles. *Nano Lett.* **11,** 4912–8 (2011).

19. Caculitan, N. G. *et al.* Size-Based Chromatography of Signaling Clusters in a Living Cell Membrane. *Nano Lett.* (2014). doi:10.1021/nl404514e

20. Lohmüller, T., Xu, Q. & Groves, J. T. Nanoscale Obstacle Arrays Frustrate Transport of EphA2-Ephrin-A1 Clusters in Cancer Cell Lines. *Nano Lett.* **13,** 3059–3064 (2013).

21. Lohmüller, T. *et al.* Single molecule tracking on supported membranes with arrays of optical nanoantennas. *Nano Lett.* **12,** 1717–21 (2012).

22. Acuto, O., Mise-Omata, S., Mangino, G. & Michel, F. Molecular modifiers of T cell antigen receptor triggering threshold: the mechanism of CD28 costimulatory receptor. *Immunol. Rev.* **192,** 21–31 (2003).

23. Evans, E. J. *et al.* Crystal structure of a soluble CD28-Fab complex. *Nat. Immunol.* **6,** 271–9 (2005).

24. Holdorf, A. D. *et al.* Proline residues in CD28 and the Src homology (SH)3 domain of Lck are required for T cell costimulation. *J. Exp. Med.* **190,** 375–84 (1999).

25. August, A. & Dupont, B. Activation of extracellular signal-regulated protein kinase (ERK/MAP kinase) following CD28 cross-linking: activation in cells lacking p56 lck. *Tissue Antigens* **46,** 155–162 (1995).

26. Tavano, R. *et al.* CD28 interaction with filamin-A controls lipid raft accumulation at the T-cell immunological synapse. *Nat. Cell Biol.* **8,** 1270–6 (2006).

27. Yuseff, M.-I., Lankar, D. & Lennon-Duménil, A.-M. Dynamics of membrane trafficking downstream of B and T cell receptor engagement: impact on immune synapses. *Traffic* **10,** 629–36 (2009).

28. Ellis, J. H., Burden, M. N., Vinogradov, D. V, Linge, C. & Crowe, J. S. Interactions of CD80 and CD86 with CD28 and CTLA4. *J. Immunol.* **156,** 2700–9 (1996).

29. Michel, F., Attal-Bonnefoy, G., Mangino, G., Mise-Omata, S. & Acuto, O. CD28 as a molecular amplifier extending TCR ligation and signaling capabilities. *Immunity* **15,** 935–45 (2001).

30. Lenschow, D. J., Walunas, T. L. & Bluestone, J. A. CD28/B7 system of T cell costimulation. *Annu. Rev. Immunol.* **14,** 233–58 (1996).

31. Tuosto, L. & Acuto, O. CD28 affects the earliest signaling events generated by TCR engagement. *Eur. J. Immunol.* **28,** 2131–42 (1998).

32. Fathman, C. G. & Lineberry, N. B. Molecular mechanisms of CD4+ T-cell anergy. *Nat. Rev. Immunol.* **7,** 599–609 (2007).

33. Stamper, C. C. *et al.* Crystal structure of the B7-1/CTLA-4 complex that inhibits human immune responses. *Nature* **410,** 608–11 (2001).

34. Zhang, X., Schwartz, J.-C. D., Almo, S. C. & Nathenson, S. G. Crystal structure of the receptor-binding domain of human B7-2: insights into organization and signaling. *Proc. Natl. Acad. Sci. U. S. A.* **100,** 2586–91 (2003).

35. Schwartz, J. C., Zhang, X., Fedorov, a a, Nathenson, S. G. & Almo, S. C. Structural basis for co-stimulation by the human CTLA-4/B7-2 complex. *Nature* **410,** 604–8 (2001).

36. Bhatia, S., Sun, K., Almo, S. C., Nathenson, S. G. & Hodes, R. J. Dynamic equilibrium of B7-1 dimers and monomers differentially affects immunological synapse formation and T cell activation in response to TCR/CD28 stimulation. *J. Immunol.* **184,** 1821–8 (2010).

37. Linsley, P. S. CTLA-4 is a second receptor for the B cell activation antigen B7. *J. Exp. Med.* **174,** 561–569 (1991).

38. Van der Merwe, P. A., Bodian, D. L., Daenke, S., Linsley, P. & Davis, S. J. CD80 (B7-1) binds both CD28 and CTLA-4 with a low affinity and very fast kinetics. *J. Exp. Med.* **185,** 393–403 (1997).

39. Linsley, P. S. *et al.* Human B7-1 (CD80) and B7-2 (CD86) bind with similar avidities but distinct kinetics to CD28 and CTLA-4 receptors. *Immunity* **1,** 793–801 (1994).

40. Van der Merwe, P. A. & Davis, S. J. Molecular interactions mediating T cell antigen recognition. *Annu. Rev. Immunol.* **21,** 659–84 (2003).

41. Pentcheva-Hoang, T., Egen, J. G., Wojnoonski, K. & Allison, J. P. B7-1 and B7-2 selectively recruit CTLA-4 and CD28 to the immunological synapse. *Immunity* **21,** 401–13 (2004).

42. Vasu, C. CD80 and CD86 C domains play an important role in receptor binding and co-stimulatory properties. *Int. Immunol.* **15,** 167–175 (2003).

43. Thiel, M. *et al.* Efficiency of T-cell costimulation by CD80 and CD86 cross-linking correlates with calcium entry. *Immunology* **129,** 28–40 (2010).

44. Butte, M. J., Peña-Cruz, V., Kim, M.-J., Freeman, G. J. & Sharpe, A. H. Interaction of human PD-L1 and B7-1. *Mol. Immunol.* **45,** 3567–72 (2008).

45. Kupfer, A. Signaling in the immunological synapse: defining the optimal size. *Immunity* **25,** 11–3 (2006).

46. Smoligovets, A. A., Smith, A. W., Wu, H.-J., Petit, R. S. & Groves, J. T. Characterization of dynamic actin associations with T-cell receptor microclusters in primary T cells. *J. Cell Sci.* **125,** 735–42 (2012).

47. Yu, Y., Smoligovets, A. A. & Groves, J. T. Modulation of T cell signaling by the actin cytoskeleton. *J. Cell Sci.* **126,** 1049–58 (2013).

48. Hartman, N. C., Nye, J. A. & Groves, J. T. Cluster size regulates protein sorting in the immunological synapse. *Proc. Natl. Acad. Sci. U. S. A.* **106,** 12729–34 (2009).

49. Graf, B., Bushnell, T. & Miller, J. LFA-1-mediated T cell costimulation through increased localization of TCR/class II complexes to the central supramolecular activation cluster and exclusion of CD45 from the immunological synapse. *J. Immunol.* **179,** 1616–24 (2007).

50. Kato, K. *et al.* CD48 is a counter-receptor for mouse CD2 and is involved in T cell activation. *J. Exp. Med.* **176,** 1241–9 (1992).

51. Jardetzky, T. S. *et al.* Three-dimensional structure of a human class II histocompatibility molecule complexed with superantigen. *Nature* **368,** 711–8 (1994).

52. Pezeshki, A. M. *et al.* HLA-DO increases bacterial superantigen binding to human MHC molecules by inhibiting dissociation of class II-associated invariant chain peptides. *Hum. Immunol.* **74,** 1280–1287 (2013).

53. Blattman, J. N. *et al.* Therapeutic use of IL-2 to enhance antiviral T-cell responses in vivo. *Nat. Med.* **9,** 540–7 (2003).

54. Grzesiek, S., Stahl, S. J., Wingfield, P. T. & Bax, A. The CD4 determinant for downregulation by HIV-1 Nef directly binds to Nef. Mapping of the Nef binding surface by NMR. *Biochemistry* **35,** 10256–61 (1996).

55. Irvine, D. J., Purbhoo, M. A., Krogsgaard, M. & Davis, M. M. Direct observation of ligand recognition by T cells. *Nature* **419,** 845–9 (2002).

56. Newell, E. W. *et al.* Structural basis of specificity and cross-reactivity in T cell receptors specific for cytochrome c-I-E(k). *J. Immunol.* **186,** 5823–32 (2011).

57. Huang, J. *et al.* The kinetics of two-dimensional TCR and pMHC interactions determine T-cell responsiveness. *Nature* **464,** 932–6 (2010).

58. Liu, B., Chen, W., Evavold, B. D. & Zhu, C. Accumulation of Dynamic Catch Bonds between TCR and Agonist Peptide-MHC Triggers T Cell Signaling. *Cell* **157,** 357–68 (2014).

59. Li, J. *et al.* Roles of CD28, CTLA4, and Inducible Costimulator in Acute Graft-versus-Host Disease in Mice. *Biol. Blood Marrow Transplant.* **17,** 962–969 (2011).

60. Egen, J. G. & Allison, J. P. Cytotoxic T lymphocyte antigen-4 accumulation in the immunological synapse is regulated by TCR signal strength. *Immunity* **16,** 23–35 (2002).

61. Nye, J. A. & Groves, J. T. Kinetic control of histidine-tagged protein surface density on supported lipid bilayers. *Langmuir* **24,** 4145–9 (2008).

62. DeMond, A. L., Mossman, K. D., Starr, T., Dustin, M. L. & Groves, J. T. T cell receptor microcluster transport through molecular mazes reveals mechanism of translocation. *Biophys. J.* **94,** 3286–92 (2008).

63. Poirier, N. *et al.* Inducing CTLA-4-dependent immune regulation by selective CD28 blockade promotes regulatory T cells in organ transplantation. *Sci. Transl. Med.* **2,** 17ra10 (2010).

64. Shen, K., Thomas, V. K., Dustin, M. L. & Kam, L. C. Micropatterning of costimulatory ligands enhances CD4+ T cell function. *Proc. Natl. Acad. Sci. U. S. A.* **105,** 7791–6 (2008).

65. Qureshi, O. S. *et al.* Trans-endocytosis of CD80 and CD86: a molecular basis for the cell-extrinsic function of CTLA-4. *Science* **332,** 600–3 (2011).

66. Sakaguchi, S. & Wing, K. Immunology. Damping by depletion. *Science* **332,** 542–3 (2011).

67. Groves, J. T. & Kuriyan, J. Molecular mechanisms in signal transduction at the membrane. *Nat. Struct. Mol. Biol.* **17,** 659–65 (2010).

68. Betzig, E. *et al.* Imaging intracellular fluorescent proteins at nanometer resolution. *Science* **313,** 1642–5 (2006).

69. Rust, M. J., Bates, M. & Zhuang, X. Sub-diffraction-limit imaging by stochastic optical reconstruction microscopy (STORM). *Nat. Methods* **3,** 793–5 (2006).

70. Hell, S. W. & Wichmann, J. Breaking the diffraction resolution limit by stimulated emission: stimulated-emission-depletion fluorescence microscopy. *Opt. Lett.* **19,** 780 (1994).

71. Kusumi, A., Shirai, Y. M., Koyama-Honda, I., Suzuki, K. G. N. & Fujiwara, T. K. Hierarchical organization of the plasma membrane: investigations by single-molecule tracking vs. fluorescence correlation spectroscopy. *FEBS Lett.* **584,** 1814–23 (2010).

72. Lasserre, R. *et al.* Raft nanodomains contribute to Akt/PKB plasma membrane recruitment and activation. *Nat. Chem. Biol.* **4,** 538–47 (2008).

73. Slaughter, B. D., Schwartz, J. W. & Li, R. Mapping dynamic protein interactions in MAP kinase signaling using live-cell fluorescence fluctuation spectroscopy and imaging. *Proc. Natl. Acad. Sci. U. S. A.* **104,** 20320–5 (2007).

74. Campi, G., Varma, R. & Dustin, M. L. Actin and agonist MHC-peptide complex-dependent T cell receptor microclusters as scaffolds for signaling. *J. Exp. Med.* **202,** 1031–6 (2005).

75. Yokosuka, T. *et al.* Newly generated T cell receptor microclusters initiate and sustain T cell activation by recruitment of Zap70 and SLP-76. *Nat. Immunol.* **6,** 1253–62 (2005).

76. Dustin, M. L. & Groves, J. T. Receptor signaling clusters in the immune synapse. *Annu. Rev. Biophys.* **41,** 543–56 (2012).

77. Schamel, W. W. A. & Alarcón, B. Organization of the resting TCR in nanoscale oligomers. *Immunol. Rev.* **251,** 13–20 (2013).

78. Shi, Y. & Massagué, J. Mechanisms of TGF-β Signaling from Cell Membrane to the Nucleus. *Cell* **113,** 685–700 (2003).

79. Cho, W. Building signaling complexes at the membrane. *Sci. STKE* **2006,** pe7 (2006).

80. Janes, P. W. *et al.* Eph receptor function is modulated by heterooligomerization of A and B type Eph receptors. *J. Cell Biol.* **195,** 1033–45 (2011).

81. Seiradake, E., Harlos, K., Sutton, G., Aricescu, A. R. & Jones, E. Y. An extracellular steric seeding mechanism for Eph-ephrin signaling platform assembly. *Nat. Struct. Mol. Biol.* **17,** 398–402 (2010).

82. Salaita, K. *et al.* Restriction of receptor movement alters cellular response: physical force sensing by EphA2. *Science* **327,** 1380–5 (2010).

83. Grakoui, A. *et al.* The Immunological Synapse: A Molecular Machine Controlling T Cell Activation. *Science (80-.).* **285,** 221–227 (1999).

84. Lillemeier, B. F. *et al.* TCR and Lat are expressed on separate protein islands on T cell membranes and concatenate during activation. *Nat. Immunol.* **11,** 90–6 (2010).

85. Manz, B. N. & Groves, J. T. Spatial organization and signal transduction at intercellular junctions. *Nat. Rev. Mol. Cell Biol.* **11,** 342–52 (2010).

86. Yu, Y., Fay, N. C., Smoligovets, A. A., Wu, H.-J. & Groves, J. T. Myosin IIA modulates T cell receptor transport and CasL phosphorylation during early immunological synapse formation. *PLoS One* **7,** e30704 (2012).

87. Deeg, J. *et al.* T cell activation is determined by the number of presented antigens. *Nano Lett.* **13,** 5619–26 (2013).

88. Matic, J., Deeg, J., Scheffold, A., Goldstein, I. & Spatz, J. P. Fine tuning and efficient T cell activation with stimulatory aCD3 nanoarrays. *Nano Lett.* **13,** 5090–7 (2013).

89. Delcassian, D. *et al.* Nanoscale ligand spacing influences receptor triggering in T cells and NK cells. *Nano Lett.* **13,** 5608–14 (2013).

90. Lin, W.-C., Yu, C.-H., Triffo, S. & Groves, J. T. Supported membrane formation, characterization, functionalization, and patterning for application in biological science and technology. *Curr. Protoc. Chem. Biol.* **2,** 235–69 (2010).

91. Chew, L. P. Voronoi Diagram / Delaunay Triangulation. at <http://www.cs.cornell.edu/home/chew/Delaunay.html>

92. Hartman, N. C. & Groves, J. T. Signaling clusters in the cell membrane. *Curr. Opin. Cell Biol.* **23,** 370–6 (2011).

93. Jaqaman, K. *et al.* Robust single-particle tracking in live-cell time-lapse sequences. *Nat. Methods* **5,** 695–702 (2008).

94. Choudhuri, K., Wiseman, D., Brown, M. H., Gould, K. & van der Merwe, P. A. T-cell receptor triggering is critically dependent on the dimensions of its peptide-MHC ligand. *Nature* **436,** 578–82 (2005).

95. James, J. R. & Vale, R. D. Biophysical mechanism of T-cell receptor triggering in a reconstituted system. *Nature* **487,** 64–9 (2012).

96. Varma, R., Campi, G., Yokosuka, T., Saito, T. & Dustin, M. L. T cell receptor-proximal signals are sustained in peripheral microclusters and terminated in the central supramolecular activation cluster. *Immunity* **25,** 117–27 (2006).

97. Yin, Y., Wang, X. X. & Mariuzza, R. A. Crystal structure of a complete ternary complex of T-cell receptor, peptide-MHC, and CD4. *Proc. Natl. Acad. Sci. U. S. A.* **109,** 5405–10 (2012).

98. Himanen, J. P. *et al.* Architecture of Eph receptor clusters. *Proc. Natl. Acad. Sci. U. S. A.* **107,** 10860–5 (2010).

99. Xu, Q., Lin, W.-C., Petit, R. S. & Groves, J. T. EphA2 receptor activation by monomeric Ephrin-A1 on supported membranes. *Biophys. J.* **101,** 2731–9 (2011).

100. Grecco, H. E., Schmick, M. & Bastiaens, P. I. H. Signaling from the Living Plasma Membrane. *Cell* **144,** 897–909 (2011).

101. Scott, J. D. & Pawson, T. Cell signaling in space and time: where proteins come together and when they're apart. *Science* **326,** 1220–4 (2009).

102. Loose, M., Fischer-Friedrich, E., Ries, J., Kruse, K. & Schwille, P. Spatial Regulators for Bacterial Cell Division Self-Organize into Surface Waves in Vitro. *Science (80-.).* **320,** 789–792 (2008).

103. Lee, K.-H. *et al.* The Immunological Synapse Balances T Cell Receptor Signaling and Degradation. *Science (80-.).* **302,** 1218–1222 (2003).

104. Doh, J. & Irvine, D. J. Immunological synapse arrays: Patterned protein surfaces that modulate immunological synapse structure formation in T cells. *Proc. Natl. Acad. Sci.* **103,** 5700–5705 (2006).

105. Wülfing, C. & Davis, M. M. M. A receptor/cytoskeletal movement triggered by costimulation during T cell activation. *Science* **282,** 2266–9 (1998).

106. Kaizuka, Y., Douglass, A. D., Varma, R., Dustin, M. L. & Vale, R. D. Mechanisms for segregating T cell receptor and adhesion molecules during immunological

synapse formation in Jurkat T cells. *Proc. Natl. Acad. Sci. U. S. A.* **104,** 20296–301 (2007).

107. Yu, C., Wu, H., Kaizuka, Y., Vale, R. D. & Groves, J. T. Altered actin centripetal retrograde flow in physically restricted immunological synapses. *PLoS One* **5,** e11878 (2010).

108. Barda-Saad, M. *et al.* Dynamic molecular interactions linking the T cell antigen receptor to the actin cytoskeleton. *Nat. Immunol.* **6,** 80–89 (2005).

109. Hashimoto-Tane, A. *et al.* Dynein-driven transport of T cell receptor microclusters regulates immune synapse formation and T cell activation. *Immunity* **34,** 919–31 (2011).

110. Jacobelli, J., Chmura, S. A., Buxton, D. B., Davis, M. M. & Krummel, M. F. A single class II myosin modulates T cell motility and stopping, but not synapse formation. *Nat Immunol* **5,** 531–538 (2004).

111. Ilani, T., Vasiliver-Shamis, G., Vardhana, S., Bretscher, A. & Dustin, M. L. T cell antigen receptor signaling and immunological synapse stability require myosin IIA. *Nat. Immunol.* **10,** 531–9 (2009).

112. Groves, J. T., Parthasarathy, R. & Forstner, M. B. Fluorescence Imaging of Membrane Dynamics. *Annu. Rev. Biomed. Eng.* **10,** 311–338 (2008).

113. Kaye, J. *et al.* Selective development of CD4+ T cells in transgenic mice expressing a class II MHC-restricted antigen receptor. *Nature* **341,** 746–749 (1989).

114. Burkel, B. M., von Dassow, G. & Bement, W. M. Versatile fluorescent probes for actin filaments based on the actin-binding domain of utrophin. *Cell Motil. Cytoskeleton* **64,** 822–832 (2007).

115. Wei, Q. & Adelstein, R. S. Conditional Expression of a Truncated Fragment of Nonmuscle Myosin II-A Alters Cell Shape but Not Cytokinesis in HeLa Cells. *Mol. Biol. Cell* **11,** 3617–3627 (2000).

116. Smith, A. W., Smoligovets, A. a & Groves, J. T. Patterned two-photon photoactivation illuminates spatial reorganization in live cells. *J. Phys. Chem. A* **115,** 3867–75 (2011).

117. Takács, B. *et al.* Myosin complexed with ADP and blebbistatin reversibly adopts a conformation resembling the start point of the working stroke. *Proc. Natl. Acad. Sci.* **107,** 6799–6804 (2010).

118. Smith, A., Bracke, M., Leitinger, B., Porter, J. C. & Hogg, N. LFA-1-induced T cell migration on ICAM-1 involves regulation of MLCK-mediated attachment and ROCK-dependent detachment. *J. Cell Sci.* **116,** 3123–3133 (2003).

119. Bubb, M. R., Spector, I., Beyer, B. B. & Fosen, K. M. Effects of Jasplakinolide on the Kinetics of Actin Polymerization: AN EXPLANATION FOR CERTAIN IN VIVO OBSERVATIONS. *J. Biol. Chem.* **275,** 5163–5170 (2000).

120. Otsu, N. A threshold selection method from gray-level histograms. *IEEE Trans. Syst. Man Cybern.* **9,** 62–66 (1979).

121. Cai, Y. *et al.* Nonmuscle Myosin IIA-Dependent Force Inhibits Cell Spreading and Drives F-Actin Flow. *Biophys. J.* **91,** 3907–3920 (2006).

122. Giannone, G. *et al.* Periodic Lamellipodial Contractions Correlate with Rearward Actin Waves. *Cell* **116,** 431–443 (2004).

123. Vicente-Manzanares, M., Ma, X., Adelstein, R. S. & Horwitz, A. R. Non-muscle myosin II takes centre stage in cell adhesion and migration. *Nat Rev Mol Cell Biol* **10,** 778–790 (2009).

124. Aratyn-Schaus, Y. & Gardel, M. L. Transient Frictional Slip between Integrin and the ECM in Focal Adhesions under Myosin II Tension. *Curr. Biol.* **20,** 1145–1153 (2010).

125. Sakamoto, T., Limouze, J., Combs, C. A., Straight, A. F. & Sellers, J. R. Blebbistatin, a Myosin II Inhibitor, Is Photoinactivated by Blue Light. *Biochemistry* **44,** 584–588 (2004).

126. Kovács, M., Thirumurugan, K., Knight, P. J. & Sellers, J. R. Load-dependent mechanism of nonmuscle myosin 2. *Proc. Natl. Acad. Sci.* **104,** 9994–9999 (2007).

127. Lewis, R. S. CALCIUM SIGNALING MECHANISMS IN T LYMPHOCYTES. *Annu. Rev. Immunol.* **19,** 497–521 (2001).

128. Bunnell, S. C. *et al.* T cell receptor ligation induces the formation of dynamically regulated signaling assemblies. *J. Cell Biol.* **158,** 1263–1275 (2002).

129. Lee, K.-H. *et al.* T Cell Receptor Signaling Precedes Immunological Synapse Formation. *Science (80-.).* **295,** 1539–1542 (2002).

130. Bolte, S. & Cordelieres, F. P. A guided tour into subcellular colocalization analysis in light microscopy. *J. Microsc.* **224,** 213–232 (2006).

131. Ohashi, Y., Tachibana, K., Kamiguchi, K., Fujita, H. & Morimoto, C. T Cell Receptor-mediated Tyrosine Phosphorylation of Cas-L, a 105-kDa Crk-associated Substrate-related Protein, and Its Association of Crk and C3G. *J. Biol. Chem.* **273,** 6446–6451 (1998).

132. Ohashi, Y., Iwata, S., Kamiguchi, K. & Morimoto, C. Tyrosine Phosphorylation of Crk-Associated Substrate Lymphocyte-Type Is a Critical Element in TCR- and β1 Integrin-Induced T Lymphocyte Migration. *J. Immunol.* **163,** 3727–3734 (1999).

133. Minegishi, M. *et al.* Structure and function of Cas-L, a 105-kD Crk-associated substrate-related protein that is involved in beta 1 integrin-mediated signaling in lymphocytes. *J. Exp. Med.* **184,** 1365–1375 (1996).

134. Kanda, H. *et al.* Fyn and Lck tyrosine kinases regulate tyrosine phosphorylation of p105CasL, a member of the p130Cas docking protein family, in T-cell receptor-mediated signalling. *Immunology* **97,** 56–61 (1999).

135. Sawada, Y. *et al.* Force Sensing by Mechanical Extension of the Src Family Kinase Substrate p130Cas. *Cell* **127,** 1015–1026 (2006).

136. Alexander, N. R. *et al.* Extracellular Matrix Rigidity Promotes Invadopodia Activity. *Curr. Biol.* **18,** 1295–1299 (2008).

137. Zheng, M. & McKeown-Longo, P. J. Cell adhesion regulates Ser/Thr phosphorylation and proteasomal degradation of HEF1. *J. Cell Sci.* **119,** 96–103 (2006).

138. Liu, X. *et al.* A novel ability of Smad3 to regulate proteasomal degradation of a Cas family member HEF1. *EMBO J* **19,** 6759–6769 (2000).

139. Ingber, D. E. Mechanobiology and diseases of mechanotransduction. *Ann. Med.* **35,** 564–577 (2003).

140. Levental, K. R. *et al.* Matrix Crosslinking Forces Tumor Progression by Enhancing Integrin Signaling. *Cell* **139,** 891–906 (2009).

141. Vogel, V. & Sheetz, M. Local force and geometry sensing regulate cell functions. *Nat Rev Mol Cell Biol* **7,** 265–275 (2006).

142. Engler, A. J., Sen, S., Sweeney, H. L. & Discher, D. E. Matrix Elasticity Directs Stem Cell Lineage Specification. *Cell* **126,** 677–689 (2006).

143. Li, Y.-C. *et al.* Cutting Edge: Mechanical Forces Acting on T Cells Immobilized via the TCR Complex Can Trigger TCR Signaling. *J. Immunol.* **184,** 5959 –5963 (2010).

144. Kim, S. T. *et al.* The αβ T Cell Receptor Is an Anisotropic Mechanosensor. *J. Biol. Chem.* **284,** 31028 –31037 (2009).

145. Husson, J., Chemin, K., Bohineust, A., Hivroz, C. & Henry, N. Force Generation upon T Cell Receptor Engagement. *PLoS One* **6,** e19680 (2011).

146. Reedquist, K. A. *et al.* Stimulation through the T Cell Receptor Induces Cbl Association with Crk Proteins and the Guanine Nucleotide Exchange Protein C3G. *J. Biol. Chem.* **271,** 8435–8442 (1996).

147. Gelkop, S., Babichev, Y. & Isakov, N. T Cell Activation Induces Direct Binding of the Crk Adapter Protein to the Regulatory Subunit of Phosphatidylinositol 3-Kinase (p85) via a Complex Mechanism Involving the Cbl Protein. *J. Biol. Chem.* **276,** 36174–36182 (2001).

148. Van Elsas, A., Hurwitz, A. A. & Allison, J. P. Combination Immunotherapy of B16 Melanoma Using Anti-Cytotoxic T Lymphocyte-Associated Antigen 4 (Ctla-4) and Granulocyte/Macrophage Colony-Stimulating Factor (Gm-Csf)-Producing Vaccines Induces Rejection of Subcutaneous and Metastatic Tumors Accompanied . *J. Exp. Med.* **190,** 355–366 (1999).

149. Callahan, M. K., Wolchok, J. D. & Allison, J. P. Anti-CTLA-4 antibody therapy: immune monitoring during clinical development of a novel immunotherapy. *Semin. Oncol.* **37,** 473–84 (2010).

150. Bridgeman, J. S. *et al.* The optimal antigen response of chimeric antigen receptors harboring the CD3zeta transmembrane domain is dependent upon incorporation of the receptor into the endogenous TCR/CD3 complex. *J. Immunol.* **184,** 6938–49 (2010).

151. Curran, K. J., Pegram, H. J. & Brentjens, R. J. Chimeric antigen receptors for T cell immunotherapy: current understanding and future directions. *J. Gene Med.* **14,** 405–15 (2012).

152. Tufet, M. T-cell activation: The waves behind the TGN1412 storm. *Nat. Rev. Immunol.* **8,** 322–323 (2008).

153. Müller, N. *et al.* A CD28 superagonistic antibody elicits 2 functionally distinct waves of T cell activation in rats. *J. Clin. Invest.* **118,** 1405–16 (2008).

154. Casucci, M. & Bondanza, A. Suicide gene therapy to increase the safety of chimeric antigen receptor-redirected T lymphocytes. *J. Cancer* **2,** 378–82 (2011).